DOE/PC/79903--T6

OPTICAL PROPERTIES OF FLYASH

Contract No. DE-AC22-87PC 79903

Quarterly Report for Period 1 July – 30 September 1990

Prepared for Pittsburgh Energy Technology Center

Principal Investigator Professor S. A. Self

October 1990

HIGH TEMPERATURE GASDYNAMICS LABORATORY
Mechanical Engineering Department
Stanford University

DOE/PC/79903--T6

DE91 004205

OPTICAL PROPERTIES OF FLYASH
Contract No. DE-AC22-87PC 79903
Quarterly Report for Period 1 July – 30 September 1990
Prepared for Pittsburgh Energy Technology Center
Principal Investigator Professor S. A. Seif

EXECUTIVE SUMMARY

The general aims of this research are to provide a fundamental scientific basis for the physical understanding and reliable calculation of radiative heat transfer in coal combustion systems, particularly as it is influenced by the presence of inorganic constituents deriving from the mineral matter in coal.

The work is organized under four tasks. Tasks I and ' were initiated in October 1987; Tasks III and IV were funded from October 1988.

Task 1. Characterization of Flyash: Under this heading the chemical composition and size distribution of representative flyashes are being measured by appropriate microanalytical techniques to provide information required in Task 2.

Task 2. Measurement of the Optical Constants of Slags: Under this heading measurements of the infrared optical constants (i.e., the complex refractive index $m = n - ik$) of synthetic slags are being made as a function of wavelength and temperature for controlled compositions. Particular attention will be given to the contribution of the Fe_2O_3 content and its valence state. The data is being reduced to yield formulae giving the complex refractive index over relevant ranges of wavelength and temperature, as a function of the relevant metal oxide constituents.

Task 3. Sample Calculations of the Radiant Properties of Flyash Dispersions: This component comprises various calculations to guide and evaluate the experimental work under the other three tasks.

Task 4. Measurement of the Radiant Properties of Flyash Dispersions: This bench-scale experiment is planned to compare the measured radiant properties of a dispersion of well-characterized ash with computations based on data developed under the first two tasks.

In this twelfth quarter good progress has been made in all four areas, as reported in the Quarterly Report, and summarized below.

Task 1

The ashes being characterized are samples from power plants or pilot-scale combustors derived from combustion of six of the coals selected for study under the parallel PETC program on "Transformation of Inorganic Coal Constituents in Combustion Systems."

The principal features requiring characterization are particle size and composition distributions, including correlations between size and composition. Size distributions are being measured in house by Coulter counter. Size and composition distributions are being determined by automated SEM/microprobe analysis at UNDERC. Other in-house characterization work under way includes size classification by wet sieving combined with classification by density using flotation/sedimentation techniques, low temperature ashing for the char content and magnetic separation for the magnetite content resulting from combustion of pyrite.

Size distributions for all six ashes over the range 0.5 – 60 μm have been completed using the Coulter multisizer with a technique employing two orifices to cover the whole range. A suitable technique for matching distributions using two orifice sizes was devised. The measured distribution was found to be very well represented by truncated log-normal distributions. Comparison with the size distribution from automated SEM shows some discrepancy which is still being investigated.

Micrographs of the ash samples prepared by UNDERC for automated SEM/EDX size-composition analysis revealed many agglomerates, casting some doubt on the validity of the data. A freeze-drying technique for sample preparation has been developed at Stanford which gives very well dispersed samples. The automated SEM/EDX analysis has been repeated using such samples and the results have been analyzed using statistical computer codes developed at Stanford. Ternary diagrams of the composition distributions (in color) have been prepared using software developed at Stanford. In the past quarter, automated SEM/EDX analyses have been completed and analysis of the data made for all six ashes.

In addition, density classification results have been obtained for all six ashes and compared with results from SEM analysis for composition, which, of course, determines the density. Currently, size distributions are being determined for the density-separated fractions to obtain composition/size correlations for comparison with the SEM/EDX data.

Task 2

Methods for determining the infrared optical properties of solid synthetic and natural slags at low temperatures have been established in prior work at Stanford. In the present work the main effort has been devoted to the development of suitable apparatus and

techniques for performing similar measurements on slags at temperatures to 2000K, when the slag is liquid. Basic experimental strategies have been decided and apparatus has been designed to accomplish this task. Preliminary tests at high temperatures during past quarters have resulted in the first reliable measurements of the infrared absorption of liquid slag.

Two complementary techniques involving infrared optical measurements on liquid samples of synthetic slag maintained in an electric furnace have been developed. The first, for the wavelength range 1 – 5 μm where the absorption index is low ($k \leq 10^{-2}$) employs a submerged platinum mirror to measure the absorption of thin films of slag by a double-pass technique. The second, applicable over the whole wavelength range (1–12 μm), measures the surface reflectance of the liquid slag relative to that of a cold gold mirror in an external reference path.

The first technique has been successfully used to obtain the first reliable measurements of the infrared absorption of liquid slag (at 2000 K).

Efforts have since been concentrated on developing and testing the second technique (for surface reflectivity measurements). It was determined that the quality of the data obtained is limited by the differing absorptions due to CO_2 and H_2O in the hot measurement path and the cold reference path. To eliminate this problem, the whole apparatus has been enclosed in a chamber, purged with dry nitrogen.

With this modification, good measurements of the reflectivity of synthetic slag containing 5% Fe at 1600°C were made over the whole wavelength range 1–12 μm. The data in the range 8–12 μm were reduced, using the Kramers–Kronig technique to give both the real and imaginary parts of the complex refractive index.

Possible sources of uncertainty in these measurements have been critically investigated and resolved. In particular, a problem due to contamination of a mirror by furnace gases has been identified and steps taken to eliminate it by redesign of the optical system. Also, in this quarter, reflectance measurements on liquid slags containing zero, 1%, 5%, 10% and 20% iron (as Fe_2O_3) have been completed. The results have been reduced, using Kramers-Kronig analysis to yield the real (n) and imaginary (k) parts of the complex refractive index.

Task 3

Programs have been written for Mie scattering calculations which are then convolved with input on the size and optical constants distributions for a particulate dispersion to yield the spectral scattering and absorption coefficients of the aerosol. Additionally, a program has been written to solve the radiation transfer problem for a homogeneous slab, utilizing the

exact solution method of Case's normal modes. Input for the spectral scattering and absorption coefficients from the first program allows the spectral scattering, absorption and emission properties of the slab to be computed. These can then be integrated over wavelength to yield the total radiative heat transfer characteristics of the slab.

These programs have been used to determine the importance of certain features of typical ashes for radiation transfer. These include the sensitivity of the optical/radiative properties of a flyash dispersion to (i) composition-size correlation, especially with regard to the distribution of iron oxides with particle size, and (ii) the presence of bubbles in the glassy ash particles.

This computational capability is also being used to evaluate the experimental conditions in the design of the apparatus for Task 4.

Task 4

Careful consideration has been given to the feasibility of various basic approaches for implementing the goals of this task. After evaluating various experimental techniques, a basic approach has been identified, which involves extinction measurements on flyash dispersed in suitable organic liquids. Measurements of the infrared transmission of three selected liquids have been made which confirm their suitability for this purpose. CaF2 windows for an absorption cell have been acquired and preliminary tests of a suitable cell design have been made.

During the past quarter, preliminary measurements of the extinction of flyash dispersions in CCl_4 have been made over the wavelength range 1 – 5 μm, and compared with calculations.

1.0 INTRODUCTION

This is the twelfth quarterly report under DOE contract No. DE-AC22-87PC 79903 entitled "Optical Properties of Flyash." Tasks 1 and 2 of this program were funded from 15 September 1987. Tasks 3 and 4 were funded from 15 September 1988.

The general aims of this research are to provide a fundamental scientific basis for the physical understanding and reliable calculation of radiative heat transfer in coal combustion systems, particularly as it is influenced by the presence of inorganic constituents deriving from the mineral matter in coal. Some preliminary work in this area has been carried out at Stanford in the past several years with NSF support. The present program will greatly enlarge the scope of this work.

The complete, integrated program of theoretical and experimental work comprises four separate tasks.

Task 1. Characterization of Flyash

Task 2. Measurements of the Optical Constants of Slags

Task 3. Sample Calculations of the Radiant Properties of Flyash Dispersions.

Task 4. Measurements of the Radiative Properties of Flyash Dispersions.

In Task 1, the chemical composition and size distribution of representative flyashes are being measured by appropriate microanalytical techniques to provide information required in Tasks 2 and 3.

In Task 2, measurements of the infrared optical constants (i.e., the complex refractive index $m = n - ik$) of synthetic slags are being made as a function of wavelength and temperature for controlled compositions. Particular attention is being given to the contribution of Fe_2O_3 content and its valence state. The data will be reduced to yield formulae giving the complex refractive index over relevant ranges of wavelength and temperature, as a function of the relevant metal oxide constituents.

In Task 3, sample calculations are being made for typical ash loadings, size distributions and compositions for simple geometries, with two main purposes: first, to provide insight and physical understanding of the role of flyash in radiative heat transfer in combustion systems; second, to indicate the sensitivity of the results to the characteristics of the input data. Such calculations will also be used to determine appropriate conditions and to predict the expected measured radiative properties for the experiment of Task 4.

The experiment of Task 4 is designed to critically test our ability to predict the measured spectral emittance and scattering coefficient of flyash dispersions under well-controlled laboratory conditions utilizing the optical property data developed in Task 2. Particular attention will be paid to assessing the contribution of the char component in typical ashes. Any discrepancies between calculated and measured quantities revealed by these tests will be resolved by appropriate further studies.

A more detailed description of the scope of these tasks is given below. First, however, an outline is given of the rationale for the overall approach adopted in this program.

1.1 Rationale of Overall Approach

To account for the effects of flyash in radiative heat transfer calculations requires a knowledge of the contributions of the ash to the spectral absorption (a_λ) and scattering (σ_λ) coefficients of the particulate dispersion, together with the phase function Φ_λ describing the anisotropy of the scattering. These quantities depend on the particulate loading as well as the distributions of the size and optical properties of the particles.

For a spherical particle of homogeneous, optically isotropic material, characterized by a complex refractive index $m \equiv (n - ik)$ Mie theory allows one to compute the spectral absorption ($Q_{\lambda,a}$) and scattering ($Q_{\lambda,s}$) efficiencies of the particle, as well as the phase function ϕ_λ. For randomly polarized radiation, these quantities are a function of the particle size parameter $x \equiv (\pi d/\lambda)$, and the complex refractive index $m(C, \lambda, T)$, a function of composition, wavelength and temperature.

For a monodispersion of identical spherical particles, of specified loading (i.e. number density), the particulate's contribution to the optical properties (a_λ, σ_λ and Φ_λ) of the medium are simply related to the spectral properties ($Q_{\lambda,a}$, $Q_{\lambda,s}$, ϕ_λ) of a single particle. It is also straightforward to compute the spectral optical properties of the medium for a polydispersion of spheres of identical composition, by convolving the results of Mie calculations for spheres of varying diameter (i.e. x) for fixed wavelength (and hence fixed m), with the particle size distribution (assumed given). In the case of a particulate material, like flyash, for which it is reasonable to assume that individual particles are of homogeneous composition but the composition varies from particle to particle, it is still possible to compute the spectral characteristics of the particulate dispersion by dividing the particles into an appropriate number of classes of varying composition (and hence m), each having a specified size distribution, and summing over particle classes.

In radiative heat transfer calculations, the contribution of the gas to the spectral absorption coefficient is added to that of the particles to obtain the combined optical properties of the medium on a spectral basis. These optical properties are then used as input for a radiation transfer code to calculate radiative fluxes, on a spectral basis, for a particular combustor geometry and boundary conditions. Finally, to obtain total heat transfer quantities such as the overall radiant heat flux, integrations over wavelength must be made.

The procedure, outlined above, represents the only logical approach to the computation of radiative heat transfer in flyash laden combustion gases. To implement this procedure requires, as input, a detailed characterization of the ash with respect to its size and (complex) refractive index distributions on a spectral basis.

Now, while techniques are available for determining the size distribution of powder samples, such as flyash, there are no practical means available for reliably determining the complex refractive index distribution of a complex material such as flyash either on a single particle basis, as a powder or as a dispersed aerosol. However, it is possible, using modern microanalytical techniques, specifically computer-automated SEM/EDX analysis, to determine the size and chemical composition of a heterogeneous powder on a particle by particle basis for a statistically large number of particles.

If the compositions of individual particles can be related to the complex refractive index of their material, then the characterization of a particular ash in terms of its size and composition distributions can lead to the necessary input for carrying out the calculations, outlined above, to compute radiation transfer in combustion systems containing that ash.

Thus the key requirement, necessary for the implementation of this approach, is data on the optical constants (i.e. the components n, k of the complex refractive index) as a function of composition, wavelength and temperature covering the range of compositions found in representative ashes. Since, as noted above, and emphasized in texts on the optical properties of particulate matter, it is impractical to extract reliable data on the optical constants of material in particulate form, the only viable approach is to make measurements on homogeneous bulk samples for which well-established techniques are available.

The foregoing arguments provide the rationale for the present program. Characterization of representative flyashes concerning their size and composition distributions constitutes Task 1, while measurements of the optical constants on bulk samples of synthetic slags as a function of relevant ranges of composition, wavelength and temperature constitute Task 2. Task 3 is designed to provide computational capabilities to support the other tasks, while Task 4 is planned to provide an experimental test that the measured optical properties of a dispersion of flyash can indeed be computed reliably from a knowledge of the size and composition distributions of the ash.

1.2 Description of Tasks

TASK 1 - Characterization of Flyash

Extensive prior analyses of flyash from a wide range of coals plus analyses of the mineral matter in raw coals, together with knowledge of the transformation processes occurring during combustion, lead to the following overall picture of the nature of flyash.

The particle size distribution is very broad with a volume (or mass) mean diameter on the order of 10 μm. Typically it is well represented by a log normal distribution with the 1% and 99% sizes in a cumulative plot by volume occurring at ~1 μm and 70 μm respectively. Evidence of a distinct submicron fume due to homogeneous condensation of volatile mineral matter is sometimes found, but this fraction can be expected to contribute negligibly to radiation transfer.

With regard to chemical composition, several distinct classes of particle can be identified and plausibly related to their origin and formation mechanisms.

By far the preponderant class, usually representing on the order of 90% or more of the ash on a mass basis, consists of vitreous (amorphous) material composed primarily of SiO_2, Al_2O_3, CaO and MgO, usually in that order, but containing varying smaller percentages of other metal oxides, notably Fe_2O_3. It can appropriately be identified as particles of impure (calcium) aluminosilicate glass derived from the microscopic clay-like mineral inclusions in the coal matrix. As char burnout proceeds these inclusions melt and form liquid globules on the surface of the char (which they do not wet) and are then released into the gas.

These glassy particles tend to be quite spherical with smooth surfaces and of reasonably homogeneous composition as is to be expected from their formation as liquid droplets. As they cool after release from the char surface, they remain in the vitreous state because the cooling rate is much faster than the crystallization rate for the formation specific phases. The fact that the bulk of most ashes consists of reasonably spherical, homogeneous and vitreous (and therefore optically isotropic) particles is a very fortunate fact, since they satisfy the assumptions of the Mie theory remarkably well.

Micrographs of optically polished sections of ash cast in epoxy resin, shows that these glassy particles sometimes contain a number of small bubbles of gas evolved from the char and trapped in the particles as they form on the char surface. More rarely, large, thin-walled cenospheres are observed which presumably are "glass-blown" when a liquid drop covers a pore in the char from which a relatively large volume of gas is evolved under pressure. Although such cenospheres are very prominent objects in micrographs, their number is usually too small to significantly affect radiation transfer.

Auger spectroscopic studies of ash often show a thin surface layer composed of volatile metals and high in sulfur (as sulfates) and water. The presence of a thin layer of adsorbed water containing sulfate ions controls the electrical resistance of the surface which is very important in the performance of electrostatic precipitators. However, this surface layer, of different composition from the underlying particle, is too thin (≤100Å) relative to wavelengths of interest to affect the optical properties of the particle.

Apart from this major class of glassy particles, several distinct minor classes of particle types can be identified, each comprising, at most, a few percent by mass of the flyash. One such class consists of incompletely burned char particles which are clearly identified in optical and SEM micrographs by the fact that they are black, of irregular shape and porous. The mass fraction of char depends on the particular coal and the combustor configuration and operating conditions. In modern combustors the mass fraction of unburned char is normally a few percent at most.

Another minor class consists of particles of adventitious incombustible mineral matter (e.g. quartz) which is contained in the pulverized coal feed. Such particles are usually large and of irregular shape, often showing rounded edges indicating partial melting.

A third minor class consists of magnetite (Fe_3O_4) which derives from the combustion of pyrite (FeS_2) particles contained in the coal grind. These magnetite particles are black, generally spherical, magnetic and much denser than the glassy particles. The proportion of magnetite particles depends on the coal type, being largest in high sulfur coals, because the sulfur is mostly associated with pyrite. Recent work has shown that much of the pyrite in the coal grind can be removed by washing/sedimentation with a reduction in SO_x emissions as high as 50% in some high sulfur coals.

The ashes selected for characterization are samples from power plants or pilot-scale combustors derived from the same seven coals selected for study under the parallel PETC program on "Transformation of Inorganic Coal Constituents in Combustion Systems" which comprise four bituminous, one sub-bituminous and two lignite coals.

A variety of techniques are being used in the characterization of these ashes. The principal method for determining size distributions employs a Coulter Multisizer which is capable of giving accurate, reliable results of high resolution over a wide dynamic range ≤1 μm to ≥ 100 μm.

Automated, computer-controlled, combined SEM/EDX microanalysis will be the principal technique used to determine the distributions of composition and size for a large number (~1000) of particles for each ash. The size distributions will be compared with those obtained by the Coulter counter.

Other techniques to be used include classification by density using liquids of varying density in a centrifuge, together with classification by size using a wet-sieving method. These techniques can yield density and size separated fractions for further examination by microanalytical techniques such as energy-dispersive X-ray spectroscopy. In addition, the magnetite particles may be separated by magnetic separation. The char content will be determined by low temperature ashing.

TASK 2 - Measurements of Optical Constants of Synthetic Slags

This task is planned to provide the basic optical properties data in a comprehensive and conveniently usable form. The optical constants (i.e., the components of the complex refractive index $m = n - ik$) of samples of synthetic slags of controlled compositions will be measured using established techniques involving transmission and surface reflectance methods. The wavelength range will extend from the visible to 12 μm, and the temperature range will extend to 2000K.

In earlier work at Stanford, supported by NSF, extensive measurements of this type were made on polished wafers of synthetic slags at temperatures up to 1200 K. A major component of this task will be to extend such measurements to higher temperatures (~2000 K) where the slag is liquid. This requires the development of modified techniques which present a number of more or less severe technical challenges.

Initially, the optical constants of the basic calcium-aluminosilicate host glass will be determined for the composition range defined by Task 1. Subsequently, by adding infrared-active mineral oxide constituents in controlled amounts, one at a time, the modifications to $m(\lambda, T)$ produced by such constituents will be quantitatively determined. The particular constituents (and their range of mass fractions) to be examined will be determined by those disclosed by Task 1, taking account of knowledge of the optical activity at relevant wavelengths of such additions from the literature of glass technology. Specific constituents to be examined will include Fe_2O_3, taking especial account of its valence state (Fe^{2+}/Fe^{3+} ratio), and of TiO_2. The contribution of the OH radical to the optical properties will be evaluated and quantified if significant.

The experimental data on $m(\lambda, T)$ as a function of composition, over the range relevant to coal ashes, will be reduced to generate simple correlation formulae. The latter will constitute the data base necessary to calculate the radiative properties of bulk slags and ash dispersions required for understanding and computing radiative transfer in coal combustion systems.

TASK 3 - Sample Calculations of the Radiant Properties of Flyash Dispersions

This task is intended to provide computational capabilities to support the other tasks. It includes the following components.

(i) A Mie scattering code to calculate the absorption and scattering efficiencies and phase function of a single sphere of specified size parameter and complex refractive index. A modified Mie code will also allow such computations for hollow spheres.

(ii) A code to convolve the results from (i) over a specified size distribution and loading to compute the absorption and scattering coefficients and phase function of a homogeneous polydispersion.

(iii) A code to sum the results of (ii) for a number of classes of particles of varying refractive indices and size distributions, i.e. for a heterogeneous polydispersion.

(iv) A radiation transfer code to calculate the absorption, scattering and emission characteristics of a homogenous, isothermal slab of dispersed ash on a spectral basis.

(v) A code to integrate the spectral results from (iv) over wavelength to yield the total radiative properties of the slab.

Calculations using these codes will be used to provide sensitivity analyses to guide the characterization work of Task 1, and to design and evaluate the results of Task 4.

TASK 4 - Measurement of the Radiative Properties of Flyash Dispersions

The purpose of this laboratory scale experiment is to test our ability to predict the measured radiative properties of a dispersion of well-characterized flyash. As such it will provide a critical test of the effectiveness of the overall approach adopted in this program.

2.0 PROGRESS IN THE PAST QUARTER

2.1 Task 1: Characterization of Fly Ash

Most of the work involved in the physical and chemical characterization of the six fly ashes has been completed. Electron microprobe analyses for the chemical composition of four of the slags, prepared by melting the fly ashes, were presented in the last QPR. The remaining two were studied this quarter and the results are discussed in the next two paragraphs. It was decided last quarter that the density classified ashes would also be sized using the Coulter Multisizer. The measurements are in progress and complete results will be reported in the next QPR. Some statistical analyses of the CCSEM data (see earlier QPRs) will also be completed next quarter.

For reasons described in the previous QPR (Task 2, page 30), the Eagle Butte slag was prepared by melting the ash in a platinum crucible for a total period of sixteen hours. The microprobe sample was obtained by core-drilling the slag. The procedure for preparing Illinois #6 ash was more complicated. As described on page 8 of the QPR dated April, 1990, the iron in the slag separated as a large pellet at the bottom of the crucible. It was suspected that reducing substances in the ash, primarily iron pyrite and some char, were responsible for removing the oxygen from the molten iron oxides. It was deemed necessary to oxidize the pyrites and char before the ash was completely molten. The fly ash sample, of mass 50 gm approximately, was first dried in hot air and then degassed under low vacuum. The ash in the alumina crucible was subsequently heated in the furnace to 1000°C. The furnace temperature was maintained at this value for a period of forty-eight hours. On cooling and weighing, the ash sample, which was now a fused mass, was found to have undergone a loss of 18.4% of its original mass. It was assumed that all the volatiles had oxidized. The sample was reheated to 1550°C and held at that temperature for eight hours. The slag, on cooling, appeared very homogeneous and glassy and did not show any further loss of mass. No iron pellet was deposited at the bottom of the crucible. Two sections of the slag from different regions were used to prepare the microprobe sample.

In Table 1, the bulk compositions of the Illinois #6 and Eagle Butte ashes, obtained using different methods, are shown together for comparison. In column 1, the composition data from CCSEM is combined with the size distribution obtained using the Multisizer to produce a bulk composition. The number of particles analyzed by CCSEM are shown in parentheses. The second column contains the microprobe results. The final column shows the composition data presented by the PSI,Inc. group [Reference 1]. Although the accuracy of the CCSEM data is limited by statistics because relatively few ash particles are analyzed, the composition distribution compares quite well with those obtained by the other techniques.

Little sulfur was detected in the microprobe study because it was oxidized and escaped as vapor during slag preparation. As observed in the previous QPR, the CCSEM study shows consistently lower iron content for all the ashes. The reason is that the large magnetite particles with high iron content that are relatively few in number were not detected. The unusually high percentage of calcia in the Eagle Butte ash is confirmed by all three sets of data.

A melt of Beulah cyclone ash was prepared for comparison with the baghouse ash. The Beulah ash is unique in that it is the only ash with almost equal proportions of alumina and silica, although it is only the absolute percentage of silica that is significant from an optical property point of view. As seen in Table 2, the cyclone ash has a higher percentage of alumina, which is not unexpected, because particles high in alumina would be heavier and collected more efficiently in the cyclone. The cyclone ash also contains significantly less iron, which is more difficult to explain. It is possible that due to low cyclone efficiency, many of the large iron-rich magnetite particles escape to the baghouse. In Task I, we have restricted complete characterization to baghouse ashes only. However, it was important to verify that the average composition of the cyclone ash was not dramatically different from the baghouse ash. We are now satisfied that baghouse ashes are quite close in average composition to the whole ashes.

Table 1: Comparison of chemical compositions of bulk fly ashes.

	Illinois #6			**Eagle Butte**		
	CCSEM (1029)	Microprobe	PSI	CCSEM (1887)	Microprobe	PSI
SiO_2	57.68	49.39	46.1	25.58	28.53	28.4
Al_2O_3	14.65	21.09	18.0	20.71	17.44	15.5
Fe_2O_3	10.01	18.96	20.5	2.82	6.88	6.1
CaO	2.38	2.94	5.3	34.22	33.0	26.4
MgO	0.14	0.9	0.6	7.53	7.47	6.2
Na_2O	0.19	1.44	1.3	1.24	1.74	2.0
K_2O	2.75	2.14	2.1	0.29	0.00	0.2
Cl	0.34	0.64	N.A.	0.46	1.05	N.A.
TiO_2	1.41	0.68	0.9	1.56	1.11	0.9
SO_3	9.37	0.02	4.4	4.41	0.01	13.7
P_2O_5	0.27	0.19	0.1	0.40	0.57	0.7
BaO	0.81	1.58	N.A.	0.79	2.5	N.A.

Table 2: Microprobe composition measurments of bulk ashes (Continued).

	Beulah Baghouse	**Beulah Cyclone**
SiO_2	31.71	29.70
Al_2O_3	33.52	38.73
Fe_2O_3	16.89	9.31
CaO	7.56	11.43
MgO	3.37	2.42
Na_2O	6.68	4.87
K_2O	1.49	1.01
Cl	0.02	0.55
TiO_2	0.67	0.21
SO_3	0.01	0.03
P_2O_5	0.39	0.59
BaO	0.62	1.16

2.2 Task 2: The Optical Properties of High Temperature Slag

The immediate goal of this task is to measure the high temperature optical properties of coal slag. The complex refractive index, $m = n + ik$, is being measured for synthetic slags at high temperatures, near 1900 K. The effect of composition on the optical properties is also being investigated.

In previous QPR's, measurements of the near normal reflectance of five synthetic slag compositions were reported (SA00, SA01, SA05, SA10, and SA20). From those measurements the complex refractive index, m, was computed using the Kramers–Kronig relations, with n being determined for the wavelength range $1 < \lambda < 13\mu m$ and k being determined for a narrower range ($8 < \lambda < 13\mu m$).

During the past quarter, a glassy slag was produced from Eagle Butte fly ash and reflectance measurements were made at approximately 1600°C. Reflectance measurements for the SA05 slag were repeated in an attempt verify the low reflectance measurements reported in the previous QPR. The previously reported SA05 data is believed to be slightly in error do to poor alignment of the optical system. The new data are presented.

2.2.1 Eagle Butte Slag Reflectance Measurements

The composition of most (by volume) of the fly ash particles analyzed under Task 1 are composed of SiO_2 and Al_2O_3, smaller amounts of CaO, Fe_2O_3 and MgO, and other trace constituents. For a major fraction of the ash volume the compositions of the particles fall, to good approximation, within the range of compositions spanned by the SAxx slags. However, the San Miguel ash is an exception since most of its particles are rich in CaO and have low levels of SiO_2 (refer to Fig. 11 in section 2.3.3). While most of the ashes contain particles with more than 30-40 wt.% SiO_2, most (> 70% by volume) of the particles in the Eagle Butte ash contain less than 30 wt.% SiO_2. The Beulah ash also has relatively low SiO_2 levels, with only half the ash volume having more than 30 wt.% SiO_2. Therefore, to determine how these low SiO_2 levels affect the optical constants, a slag was produced from the San Miguel fly ash and reflectance measurements were made.

Initial melts of the San Miguel ash were very troublesome since the ash apparently has a low melting temperature and dissolved the alumina crucible containing the melt. To overcome this problem a platinum crucible was purchased in which to make the Eagle Butte melt (named NAEB, **N**atural slag produced in **A**ir from **E**agle **B**utte ash). The platinum crucible is approximately 65mm in diameter and 20mm deep. To produce the NAEB slag the crucible was filled with Eagle Butte ash and heated in the electric furnace at ~1550°C for 8 hours. This produced a depth of approximately 5mm of solid slag in the crucible – not enough for transmittance measurements. Therefore, the crucible was filled again with ash and heated at ~1550°C for another 8 hours. This produced approximately 1 cm of slag in the crucible, which is a sufficient depth for transmittance measurements.

The resulting slag was not glassy and appeared to have a greenish-brown surface layer. Initially this layer was suspected to be due to minor species forming a film on top of the slag. If there is a surface layer, then the reflectance measurements would not produce reliable information about the optical constants of the bulk slag. Therefore, the crucible was submerged in undiluted hydrofluoric acid for several hours to dissolve the top layer. The crucible was then cleaned and placed in the furnace for another 8 hours at ~ 1500°C. The resulting slag appeared unchanged. Core samples obtained from the crucible revealed a glass beneath the rough surface. It was finally concluded that the rough surface was do to crystal formation. This conclusion was confirmed by cooling the slag quickly by quenching in room air. The increased cooling rate did not allow crystal formation and a clean glassy slag surface resulted.

The reflectance of the NAEB slag was measured with the slag at ~ 1600°C. The results are shown in Fig. 5, along with reflectance measurements for the SAxx slags. The reflectance of the NAEB slag is larger than that of the SAxx slags at wavelengths shorter than 8.5 μm, and is lower at longer wavelengths. However, the qualitative shape of the reflectance curve is the same for all of the slags. It is apparent that the SiO_2 vibrational absorption peak is shifted to longer wavelengths for the low SiO_2 NAEB slag.

The Kramers–Kronig relations were used to obtain the real refractive index, n, over the entire wavelength range $1 < \lambda < 13$ μm and to determine k at wavelengths where $k > 0.1$. Results of the analysis are shown in Fig. 6 and Fig. 7.

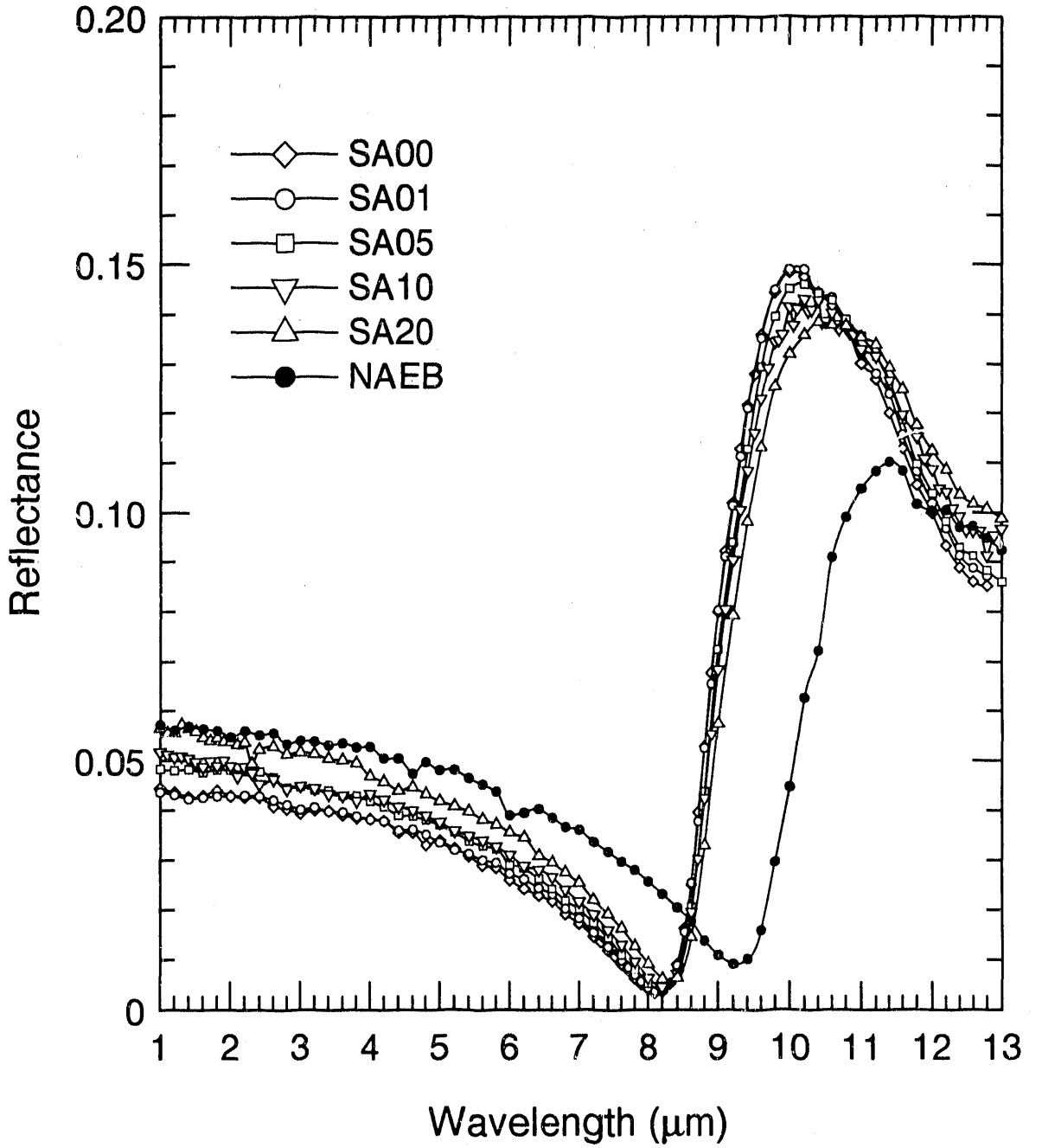

Figure 5: Near normal reflectance of several molten slags, including the slag NAEB produced from Eagle Butte fly ash.

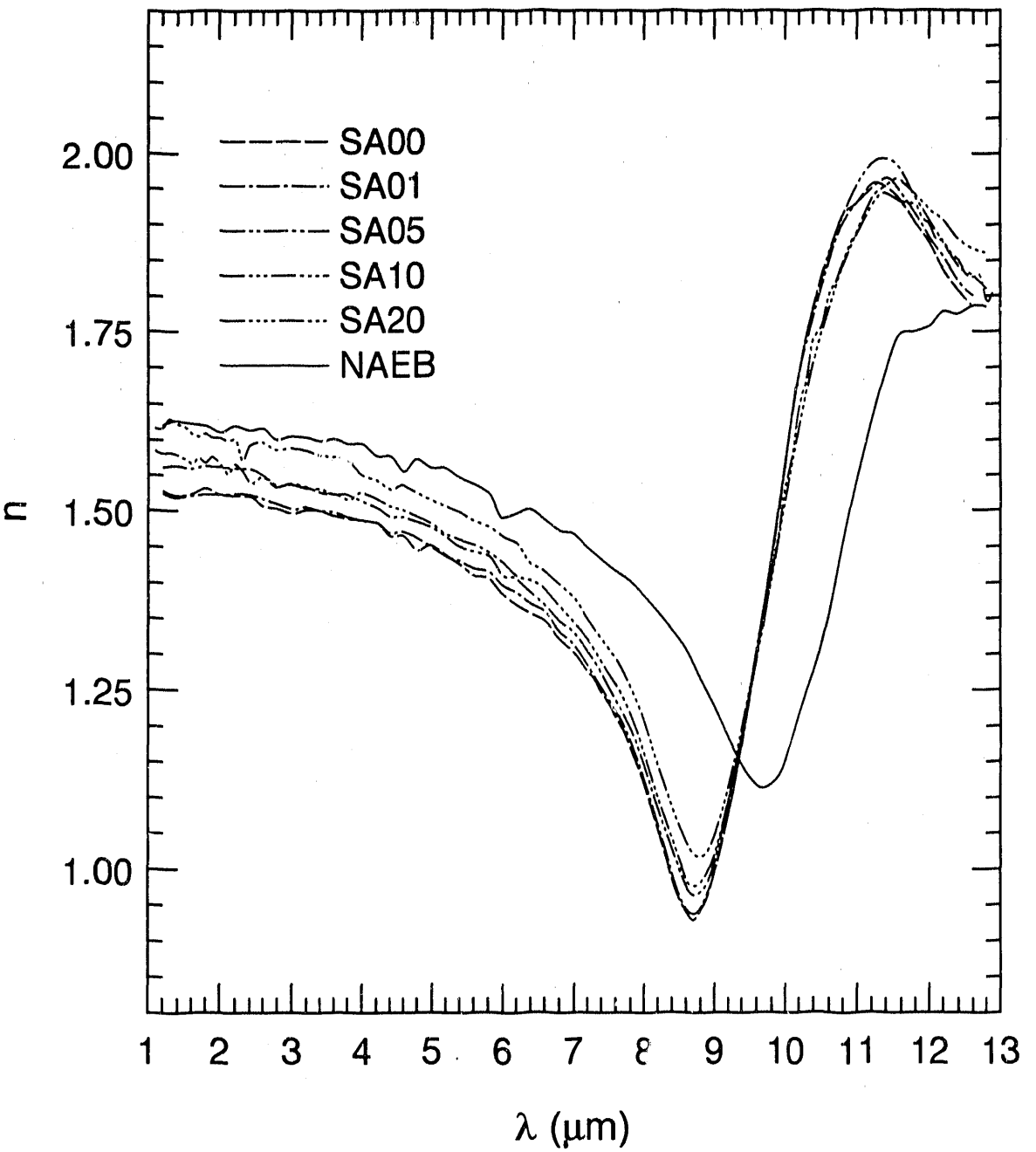

Figure 6: Real refractive index, n, of several molten slags, including the slag NAEB produced from Eagle Butte fly ash.

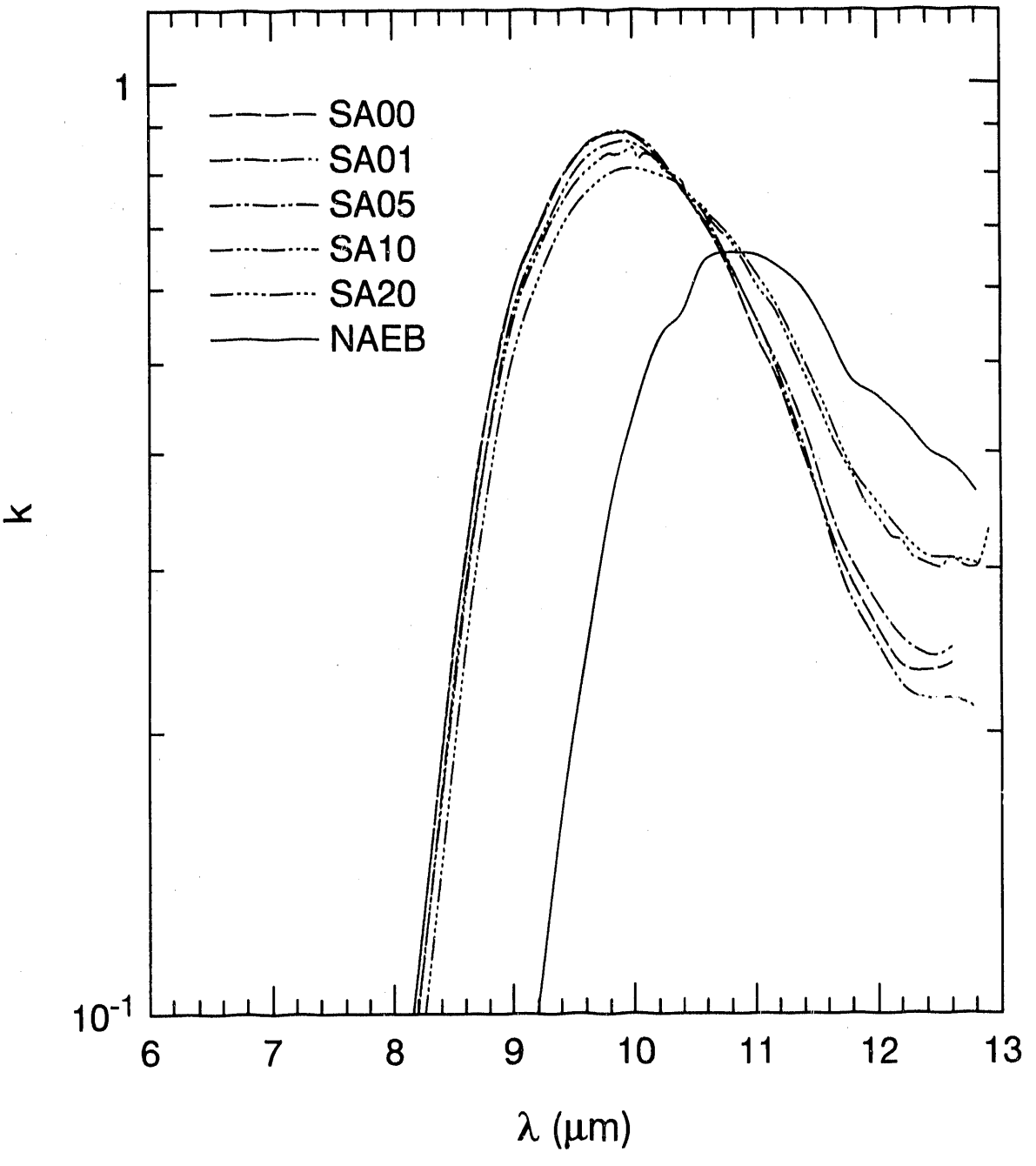

Figure 7: Absorption index, k, of several molten slags, including the slag NAEB produced from Eagle Butte fly ash.

The real refractive index, n, for molten NAEB slag ($T \sim 1600°C$) follows the trend shown in the reflectance data closely, as expected. The refractive index is larger for NAEB than for SAxx slags at shorter wavelengths (below $\sim$ 9.5 μm) and smaller at longer wavelengths. The minimum near 9.8 μm is much larger than the minimum of the other slags, and occurs at a longer wavelength. In general, the trend is consistent for all the slags, with the minimum n increasing and shifting to longer wavelengths as the SiO_2 content is decreased. However, the NAEB slag is more dramatically shifted than even SA20, which has approximately 46 wt% SiO_2, compared to approximately 20 wt.% SiO_2 for NAEB. The imaginary refractive index, k, shown in Fig. 7, shows that the peak absorption has shifted from approximately 10 μm for the SAxx slags to approximately 11 μm for the NAEB slag.

The above trend is most easily seen in the complex dielectric function, $\epsilon = m^2 = (n^2 - k^2) + i2nk$, shown in Fig. 8. As the weight percentage of SiO_2 decreases from approximately 58% for SA00 to approximately 20% for NAEB the peak in $2nk$ moves from approximately 10.1 μm to 11.2 μm. The dielectric function is a particularly useful way to present optical constants since it makes simple harmonic oscillator fits, based on microscopic properties of the matter, simpler to interpret. For example, the Lorentz oscillator model for a single damped harmonic oscillator is results in the relation

$$\epsilon = 1 + \frac{\omega_p^2}{\omega_0^2 - \omega^2 - i\gamma\omega} \tag{1}$$

where ω is frequency ($\sim 1/\lambda$), ω_p is the plasma frequency, ω_0 is the fundamental oscillator frequency, and γ is the damping constant. The peak in the imaginary part of ϵ has a value of $\omega_p^2/\gamma\omega_0$ and is at a frequency near ω_0.

To further investigate the effect of SiO_2 content on the optical constants in the 8-13 μm region, a single oscillator fit in the form of Eq. (1) was fitted to the measured reflectance data, using only data in the 8-13 μm wavelength range. The formula for the fit was modified to account for higher frequency oscillators by using the form

$$\epsilon = n_\infty^2 + \frac{\omega_p^2}{\omega_0^2 - \omega^2 - i\gamma\omega} \tag{2}$$

where n_∞ is a real constant that allows the high frequency dielectric function to approach a constant other than unity. The fit was found by allowing all four of the constants in Eq. (2) to vary in a systematic fashion (simplex method) until the RMS error was minimized. Since raw data were used, the fits are not always equally weighted

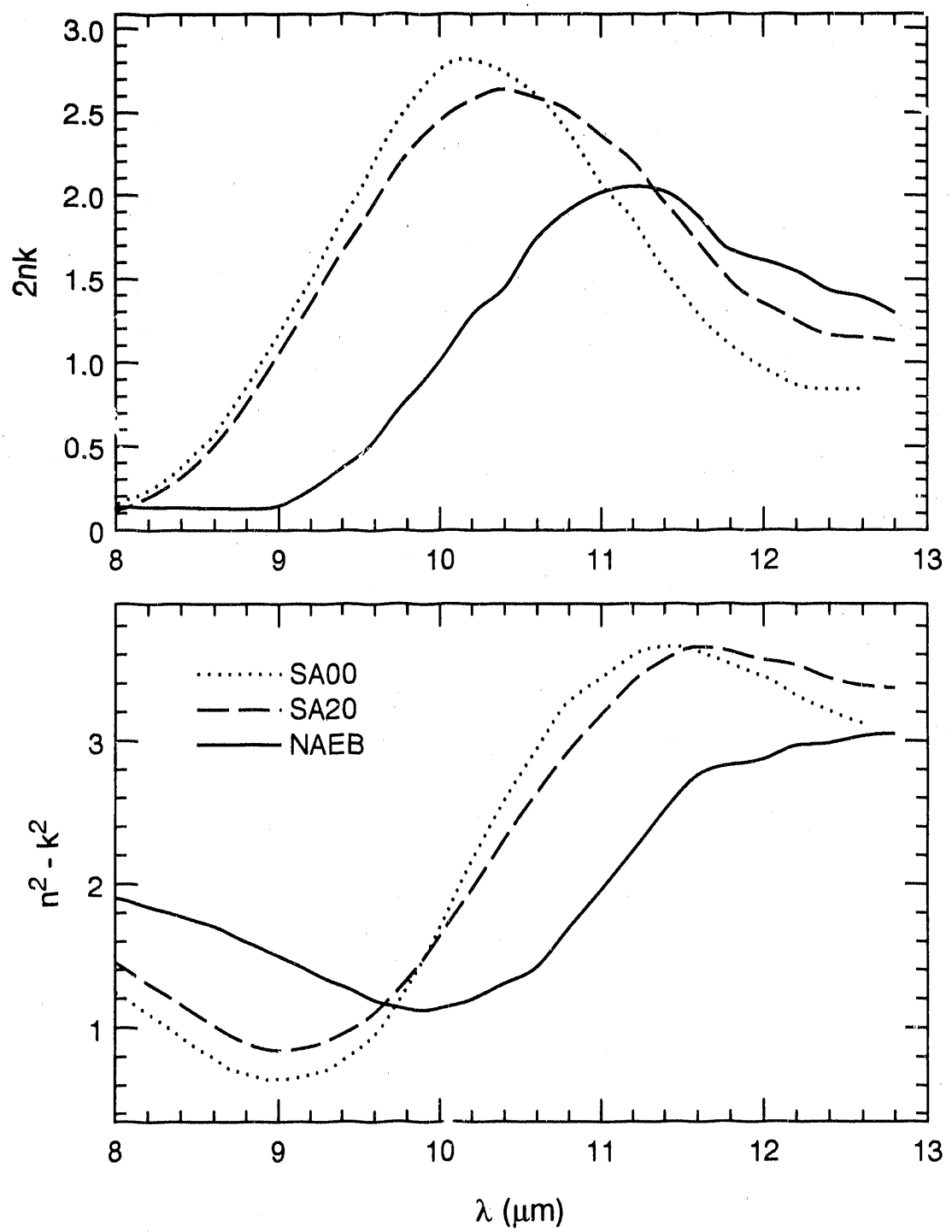

Figure 8: Complex dielectric function for molten SA00, SA20, and NAEB slags.

in frequency (or wavelength) since the raw data for some slags are at smaller wavelength increments in certain wavelength regions than others (Perhaps a better scheme would be to use an interpolating cubic spline to generate data at uniform frequency intervals).

Table 1: Parameters for single Lorentz oscillator fits

Slag	SiO_2 wt.%	n_∞	$\omega_p(1/\text{cm})$	$\omega_0(1/\text{cm})$	λ_0 (μm)	$\omega_p^2/\gamma\omega_0$
SA00	58	1.37	766	980	10.20	2.88
SA01	57	1.38	772	980	10.20	2.90
SA05	55	1.35	774	965	10.36	2.82
SA10	52	1.41	793	974	10.27	2.74
SA20	46	1.40	796	958	10.44	2.71
NAEB	20	1.48	592	908	11.01	2.04

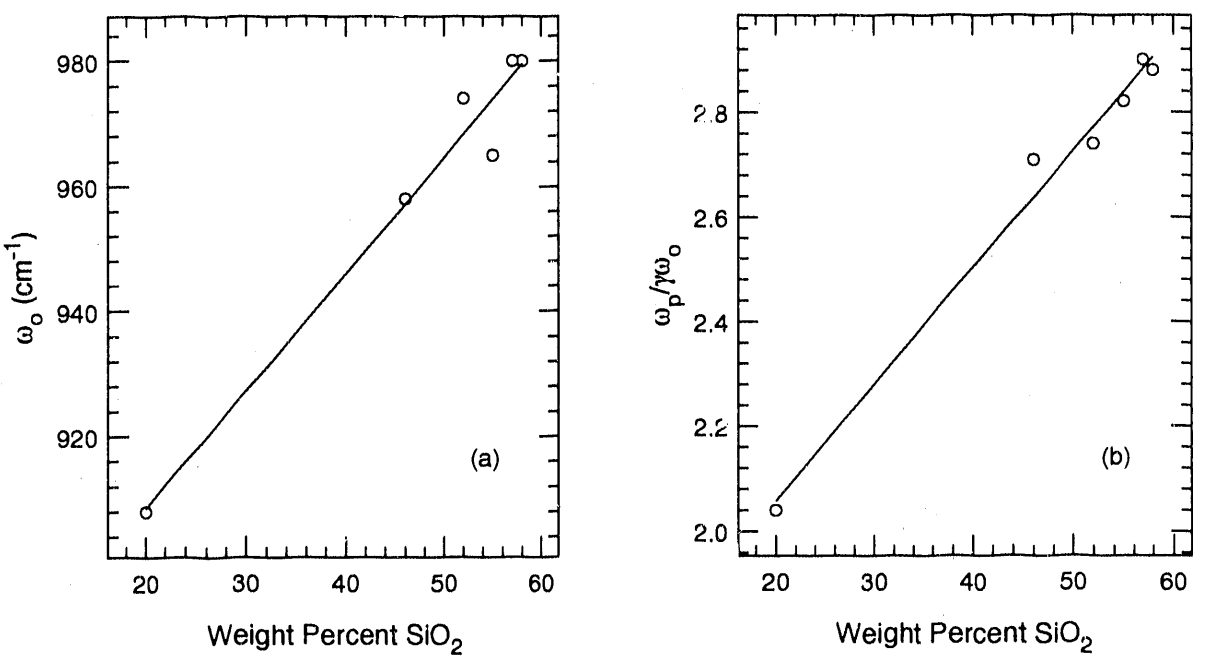

Figure 9: Frequency ω_0 (a) and maximum value of $2nk$ for single oscillator fits versus SiO_2 content.

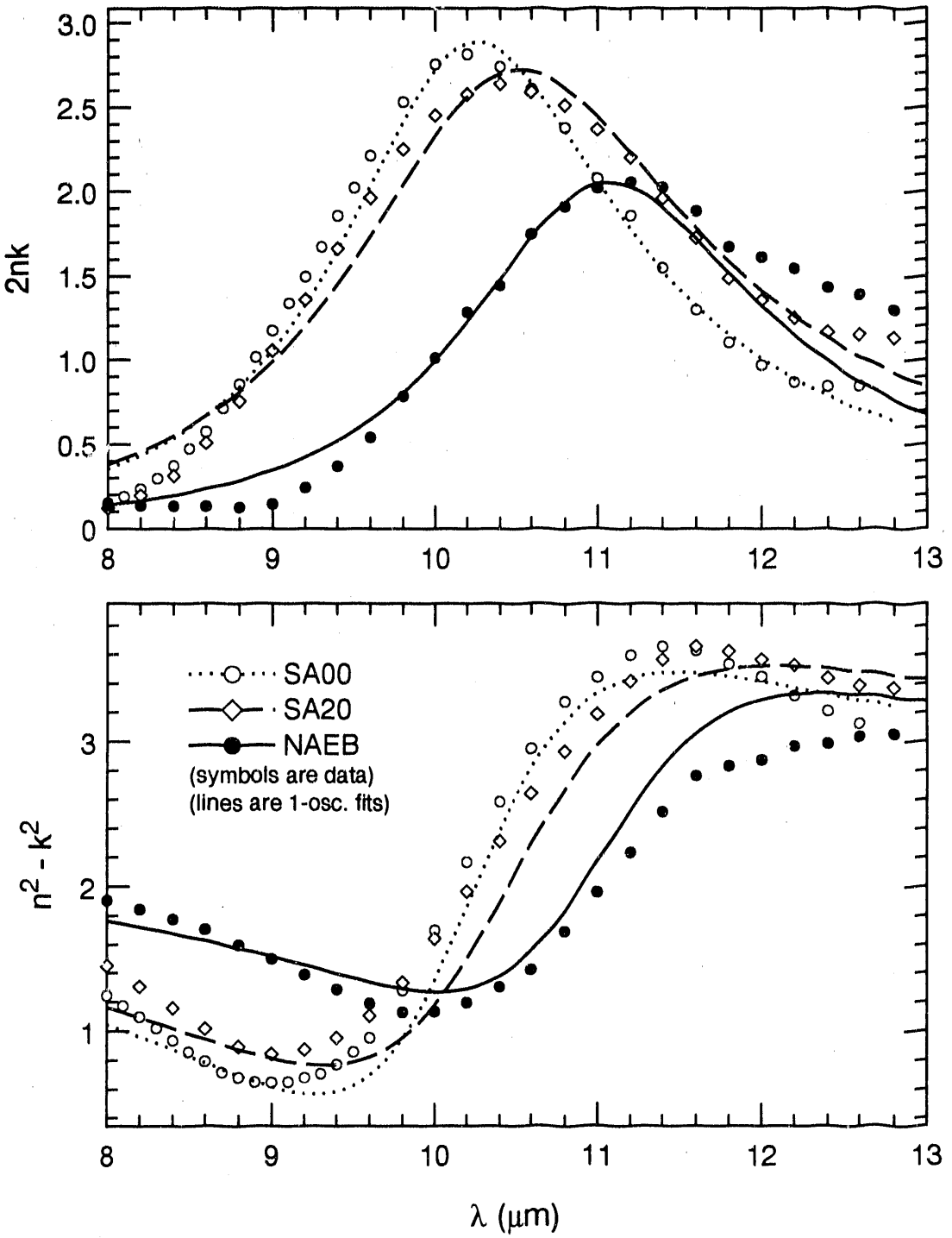

Figure 10: Comparison of single oscillator fit to measured data for three slags with varying SiO_2 contents. The symbols are data and the lines are the fit.

Figure 10 shows experimental data and oscillator fit versus wavelength for three slags. The fits are reasonably good, although the absorption process is clearly more complicated than can be represented by just a single harmonic oscillator. The fit for SA00 slag has an oscillator position, ω_0, at 980 cm^{-1}, which is near the expected position of 956 cm^{-1} for stretching vibrational absorption by Si-O^- found by Goodwin [4] for room temperature slags and for silicate glasses containing high levels of alkali oxides [1-3]

The fit parameters are shown in Table 1 and corresponding plots of the oscillator frequency ω_0 and peak absorption are shown in Fig. 9. The line drawn through the data seems to indicate that the absorption band position and strength are well correlated to SiO_2 content, although more data would add confidence to this presumption. It is clear that the NAEB slag is not inconsistent with the trends exhibited by the SAxx slags. Note that the low band position for SA05 is attributable to a poor fit by the single oscillator due to the data being at non-uniform frequency intervals as discussed above.

Similar trends in absorption peak position and band strength are reported by Simon [3] for silicate glasses containing varying levels of Na_2O and are explained in terms of "disordering" in the glass. It is also known [3] that decreasing the SiO_2 content and increasing the temperature have similar effects - the absorption band weakens and shifts to lower frequencies.

2.2.2 Scheduled Activities

During the next quarter several reflectance and transmittance measurements will be made. Correlations are being considered and analyzed that will allow accurate prediction of the optical constants for a large range of ash compositions, including lower SiO_2 ashes such as found in the Eagle Butte and Beulah samples. Appropriate samples of synthetic slag will be prepared.

2.3 Task 3: Sample Calculations of the Radiant Properties of Fly Ash Dispersions

The goals of this task are to provide sample calculations which allow estimates of the influence of fly ash on the total radiative heat transfer in coal combustors and provide computational capabilities required to evaluate our overall approach using results from Task 4. Therefore, a detailed model is being developed which is expected to provide a high level of accuracy. Simpler and more efficient models for incorporating ash into heat transfer codes can be developed and evaluated using this detailed model once the importance of ash on radiative heat transfer is known.

During the previous quarter, work has continued toward modeling the radiative properties of fly ash to allow investigation of the effects of fly ash on radiation heat transfer in coal combustion systems.

2.3.1 Overview

In this research program, we have adopted the approach that by measuring fundamental properties (i.e, the complex refractive index, m) of the fly ash which participates in the radiation transfer, one can use well established theoretical principles (Mie theory) to compute the radiative properties of dispersions of fly ash as found in coal combustors. With this approach one can understand the underlying principles that affect the radiative properties of an ash dispersion and more confidently predict how variations in the characteristics of the ash dispersion cause variations in its radiative properties.

An important criterion in this approach is that the fly ash particles be spherical, homogeneous, and isotropic. Fortunately, fly ash particles are formed at high temperatures at which most of them are molten, leading primarily to spherical particles. Furthermore, one should expect that molten particles will be reasonably homogeneous and isotropic. On cooling, most fly ash particles form glassy spheres which are homogeneous and isotropic, but some, and perhaps most from some types of coal, may form spheres or spheroids with interior bubbles or voids.

To the extent that some ash particles are not spherical, homogeneous, or even isotropic, one should consider departures from the simpler model as corrections. The

importance of these corrections must be weighed in light of the overall influence of ash on radiation heat transfer in coal combustors. We expect that most fly ash is well modeled as isotropic, homogeneous spheres, and that this approach goes much further toward explaining the effects of fly ash on radiative transport than other possible approaches.

2.3.2 Average Radiative Properties of Ash Dispersions

Fly ash particles vary in diameter over several orders of magnitude and the composition varies from particle to particle. Before radiation heat transfer can be computed for fly ash dispersions, average scattering and absorption coefficients must be computed.

For a given size distribution, $f(D)$, where $f(D)\,dD$ is the number fraction of particles with diameters between D and $D+dD$, the average scattering and absorption coefficients are given by

$$\sigma_\lambda = \frac{3}{2}\frac{C_v\overline{Q_{s\lambda}}}{D_{32}} \quad \text{and} \quad \alpha_\lambda = \frac{3}{2}\frac{C_v\overline{Q_{a\lambda}}}{D_{32}}. \tag{3}$$

Here $\overline{Q_{s\lambda}}$ and $\overline{Q_{a\lambda}}$ are the scattering and absorption efficiencies averaged over size distribution, D_{32} is the Sauter mean diameter defined by

$$D_{32} \equiv \frac{\int_0^\infty D^3 f(D)\,dD}{\int_0^\infty D^2 f(D)\,dD} \tag{4}$$

and C_v is the local volume of ash per unit volume of the dispersion. From previous QPRs, we know that the average efficiency (scattering or absorption) for a polydispersion is given by

$$\overline{Q_\lambda} = \frac{\int_0^\infty Q_\lambda(D)\,D^2 f(D)\,dD}{\int_0^\infty D^2 f(D)\,dD}. \tag{5}$$

The averaged scattering phase function (or it's Legendre coefficients) is found from the relation

$$\overline{\Phi_\lambda}(\theta) = \frac{\int_0^\infty Q_{s\lambda}(D)\,D^2\Phi_\lambda(D,\theta)\,f(D)\,dD}{\int_0^\infty Q_{s\lambda}(D)\,D^2 f(D)\,dD}. \tag{6}$$

In addition to averaging over particle size, the radiative properties must be averaged over composition (or optical constants) classes. Let $\overline{Q_{\lambda,i}}$ be the size averaged scattering or absorption efficiency for a composition class i of particles with a volume fraction $C_{v,i}$ and Sauter mean diameter $D_{32,i}$. The average scattering or absorption coefficient can

be expressed as the sum over all classes, i. The scattering and absorption coefficients are then

$$\sigma_\lambda = \frac{3}{2}\sum_i \frac{C_{v,i}\overline{Q_{s\lambda,i}}}{D_{32,i}} \quad \text{and} \quad \alpha_\lambda = \frac{3}{2}\sum_i \frac{C_{v,i}\overline{Q_{a\lambda,i}}}{D_{32,i}}. \tag{7}$$

The average scattering phase function is

$$\Phi_\lambda(\theta) = \frac{\sum_i \frac{C_{v,i}}{D_{32,i}}\overline{Q_{s\lambda,i}\Phi_{\lambda,i}}(\theta)}{\sum_i \frac{C_{v,i}}{D_{32,i}}\overline{Q_{s\lambda,i}}} \tag{8}$$

where $\overline{\Phi_{\lambda,i}}(\theta)$ is the size distribution averaged scattering phase function for particle class i.

2.3.3 Classification of Fly Ash

It is necessary to devise "composition" classes such that particles of like classes have similar optical properties – not necessarily the same composition. Since particles of different compositions may have similar scattering and absorption properties over specific finite wavelength ranges, this classification is not strictly based on composition.

For a real ash dispersion, the particle to particle composition variation results in a corresponding refractive index variation. However, we have seen that for a large range of compositions in which the primary constituents are SiO_2, Al_2O_3, CaO, and Fe_2O_3 (the SAxx slags) the optical constants do not vary considerably except in the wavelength range $1 < \lambda < 4\mu$m, where the absorption index k is dependent on the iron content of the slag. Since one cannot hope to measure the complex refractive index for every minor variation in particle composition, the fly ash must be grouped into composition classes for which the optical constants of its member particles are approximately constant.

The CCSEM data from UNDERC gives composition data that is useful for classification of the ash. Figure 11 shows a plot of the composition distribution for six ashes. The elemental UNDERC data was converted to oxide compositions for each of approximately 1000 particles per ash sample by assuming appropriate oxide formula. Then the particles were sorted into increasing size order and the largest 10 percent were omitted to remove the effects of poor statistical sampling of large particles. Next, the volume fraction of ash with oxide weight percent below a given level, x, was computed for SiO_2, Al_2O_3, CaO, Fe_2O_3, and the sum of these four oxides. Although this

presentation does not give the composition of any single particle, it does allow one to make a number of important observations.

Interpretation of Fig. 11 is relatively simple. Large slopes represent oxide weight percentages that are abundant, and small slopes represent less common oxide weight percentages. Zero slope indicates an absence of particles with that weight percentage. For example, very little of the Upper Freeport ash is composed of more than 10% Fe_2O_3, more than 50% Al_2O_3, or less than 40% SiO_2. Also, the Illinois #6 ash has a broader range of SiO_2 levels than the other ashes. Approximately 10% of the Kentucky #9 ash volume has less than 10% SiO_2, but very little of the ash volume has between 10 and 40% SiO_2.

Referring to Fig. 11, it is evident from the solid curve that most of the ash volume is made up primarily of Fe_2O_3, CaO, Al_2O_3, and SiO_2. For example, the Upper Freeport ash, has less than 5% of the ash particles by volume having less than 80% Fe_2O_3+CaO+Al_2O_3+SiO_2. Also, for the Upper Freeport ash, approximately half of the ash volume is due to particles with less than approximately 50% SiO_2, and approximately 10% of the ash volume is due to particles with less than 40% SiO_2. Similar trends are exhibited by the other ashes with the exception of Eagle Butte ash, which is rich in CaO.

The primary conclusion drawn from the study of Fig. 11 is that the synthetic slag compositions are similar to the compositions of a large fraction of the ash particles (by volume) analyzed. Of course, some fraction of the ash falls outside the SAxx composition range, but modeling the ash as $(1-x)58\%SiO_2$, $(1-x)29\%Al_2O_3$, $(1-x)13\%$CaO, and $100x\%Fe_2O_3$ (the SAxx slags) is probably sufficient for most of the ashes, especially in light of the weak dependence of $m(=n+ik)$ on composition over much of the wavelength range $1-13\mu$m. The primary composition variation is in the $1-4\mu$m range where k increases with increasing Fe_2O_3 content.

The Fe_2O_3 content of the six fly ashes is shown in Fig. 12 as volume fraction of ash with x weight percent Fe_2O_3 versus x. From this figure it is evident that most of the ash volume has less than $20\%Fe_2O_3$. Also shown on Fig. 12 is the volume fraction of ash with less than $25\%Fe_2O_3$ (i.e., $C_{v,0-25}/C_v$). The Illinois#6 sample has the broadest range of Fe_2O_3 content with 13% of the ash volume having more than 25% Fe_2O_3 and with the largest volume fraction (14%) of ash having 1% Fe_2O_3. The San Miguel ash

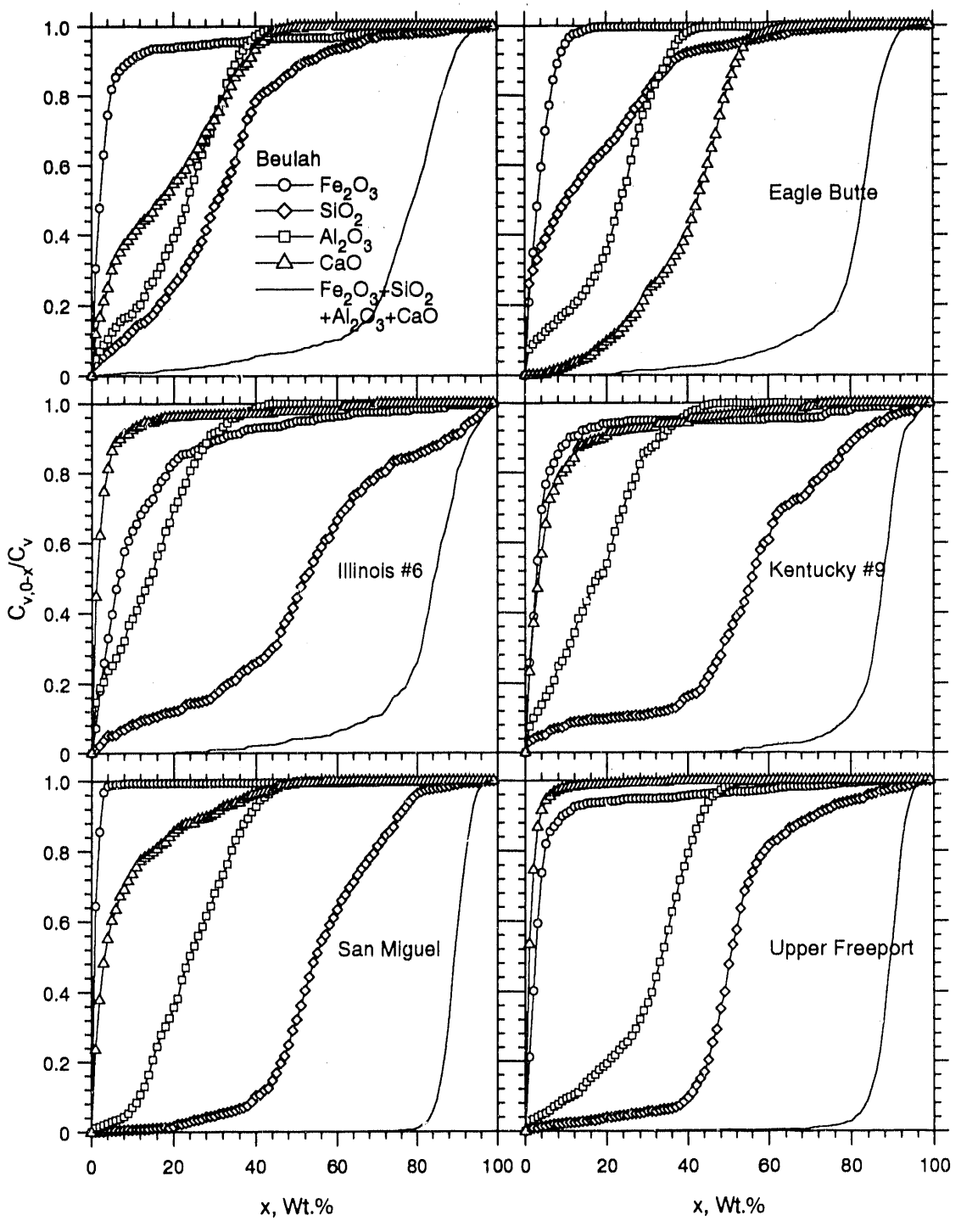

Figure 11: Volume fraction of ash with weight percent of various oxides less than x for six fly ash samples

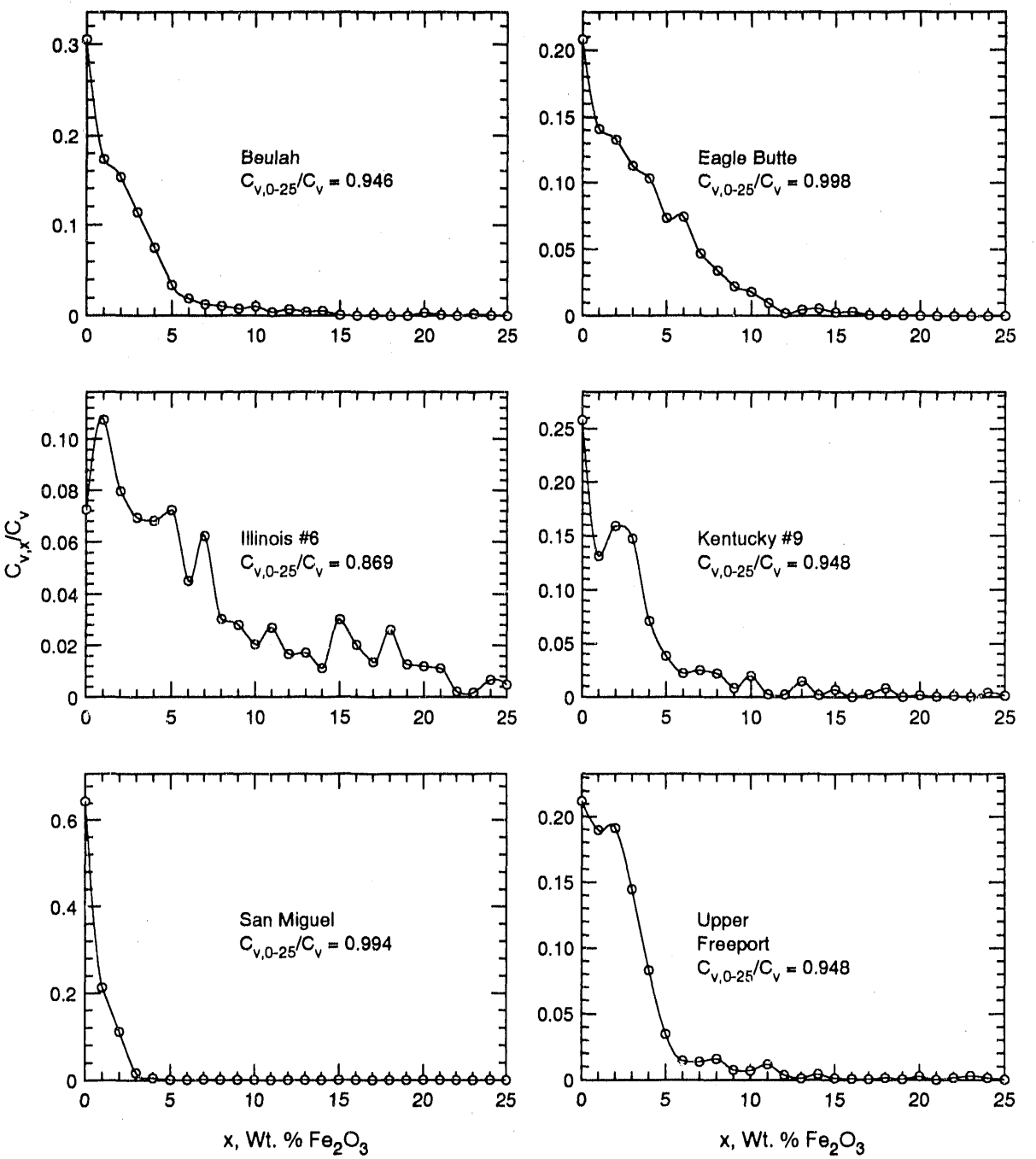

Figure 12: Ash Volume Fraction versus Fe_2O_3 weight percentage for six fly ash samples. Note differing ordinate scales.

has the least amount of iron with approximately 65% of the ash volume having less than 1% Fe_2O_3.

The above analysis of ash compositions suggests a classification scheme based on Fe_2O_3 content. In particular, assume that the ash is composed of spherical homogeneous and isotropic particles (for which Mie theory is appropriate) and that the composition is $(1-x)58\%SiO_2$, $(1-x)29\%Al_2O_3$, $(1-x)13\%CaO$, and $100x\%Fe_2O_3$ (the SAxx slags). Then use correlation formulae for the SAxx slags to obtain the optical constants ($m = n + ik$) for a given weight percent of Fe_2O_3, x, and temperature, T.

2.3.4 Correlation Formulae for the Optical Constants

Several correlation formulae have been developed for room temperature optical constants (n, k) [4] of coal slags. Three separate models are used to correlate (n, k) over the wavelength range $1 < \lambda < 13\mu$m:

1) In the wavelength range $\lambda < 7.8\mu$m the real refractive index, n, is modeled using single oscillator dispersion relations.

2) In the wavelength range $\lambda < 4\mu$m the absorption index, k, is correlated to the Fe^{2+} and total Fe_2O_3 content.

3) In the strong SiO_2 absorption region ($8 < \lambda < 13\mu$m) the complex dielectric constant, $\epsilon = m^2 = (n + ik)^2$ is modeled using a three oscillator least squares fit.

These three correlations are not completely independent since the dispersion relation for n in the near infrared is dependent on the position of the restrahlen absorption peaks at longer wavelengths (λ_0) and the strength of the oscillators in the restrahlen absorption band depend on Fe content. However, since the correlation formulae used are not complicated (or complete) enough to establish this connection, each region is analyzed and discussed separately.

Once all the data are obtained under Task 2, similar relations will be developed for the high temperatures, which should lead to temperature correlations. However, room temperature correlations are required for the evaluation of Task 4 data and are useful as a basis for further developments.

1) Near Infrared Dispersion Relations for $n\,(\lambda < 8\mu\text{m})$

Goodwin [4], following the development in Born and Wolf [5], have presented a mixture rule for n in the low absorption region $\lambda < 8\mu$m. The analysis, summarized here, is based on the Lorentz–Lorenz formula relating the mean polarizability of a material, α, to it's refractive index, n, through the relation

$$\alpha = \frac{3}{4\pi N_p}\frac{n^2-1}{n^2+2} \tag{9}$$

where N_p is the number density of atoms or molecules. Since α is, to good approximation, a property of the atom or molecule, we can approximate the average polarizability of a mixture using sums of the polarizability of it's constituents. That is,

$$\frac{n^2-1}{n^2+2} \simeq \rho \sum_i \left[\left(\frac{X_{m,i}}{\rho_i}\right)\frac{n_i^2-1}{n_i^2+2}\right] \tag{10}$$

where ρ is the density of the mixture, $X_{m,i}$ is the mass fraction of component i, ρ_i is the density of pure component i, and n_i is the refractive index of the pure component i.

The refractive index of pure component i is accurately modeled using the single harmonic oscillator model

$$n_i^2 - 1 \simeq C_i + \frac{B_i\lambda^2}{\lambda^2 - \lambda_{0,i}^2} \tag{11}$$

where C_i is a constant that corrects for neglect of higher frequency oscillators, B_i is function of the lower frequency absorption band strength, and $\lambda_{0,i}$ is the mean position of the infrared absorption peak. This model is very accurate for dielectrics in wavelength regions below strong vibrational absorption bands, e.g., in the visible to 8μm region for coal slags. Interting Eq. (11) in to Eq. (10) one obtains a mixture rule of the form

$$\frac{n^2-1}{n^2+2} \simeq \rho \sum_i \left[\left(\frac{\text{wt.\%}i}{100}\right) F_i(\lambda)\right], \quad \text{where} \quad F_i(\lambda) = \frac{a_i\lambda^2 - b_i}{c_i\lambda^2 - d_i}. \tag{12}$$

Here wavelength has units of micrometers and ρ has units of g/cm^3. The constants a_i, b_i, c_i, and d_i were found by Goodwin by minimizing the error between Eq. (12) and the room temperature synthetic slag data in the wavelength range $1 < \lambda < 8\mu$m. Table 2 gives the recommended values for six most common and abundant constituents of coal slags.

Table 2: Mixture Rule Parameters, from Goodwin [4].

Oxide	a	b	c	d
SiO_2	0.9389	53.00	5.001	420.0
Al_2O_3	1.914	174.0	10.36	1633.8
CaO	4.250	827.7	16.63	6102.3
Fe_2O_3	1.647	0.00	11.36	0.00
TiO_2	2.720	260.0	15.80	1954.4
MgO	1.278	136.9	7.433	1200.9

Finally, the density of the bulk slag, ρ, is required in Eq. (12). Goodwin found that bulk slag densities correlated well with the Fe_2O_3 content *via* the relation

$$\rho \simeq 2.524 + 0.00978\,(\text{wt.\%}Fe_2O_3)\,. \tag{13}$$

These relations for n in the $1 < \lambda < 8\mu$m wavelength range are only for room temperature slags, but we are currently studying their extension to high temperature by letting the constants a_i, b_i, c_i, and d_i be functions of temperature. Results are not yet available.

2) Absorption Index, k, in the 1-4μm range

The imaginary refractive index, k, for the base slag SA00 is very small ($< 10^{-6}$) in the wavelength range $1 < \lambda < 4$ μm. However, as the iron content is increased, absorption by Fe^{2+} ions and by intervalence charge transfer between neighboring Fe^{2+} and Fe^{3+} ions causes an increase in k. The Fe^{2+} absorption has a primary absorption band near 1.1 μm and a secondary peak centered near 2μm. The intervalence charge transfer absorption is centered at visible wavelengths but is typically a broad absorption band extending into the infrared. It is believed that this intervalence charge transfer absorption band is broadened at elevated temperatures and is chiefly responsible for the increase in k with increasing T. The ferrous iron absorption does not seem to change significantly with temperature. Thus the effect of temperature on k in this region may be quite dependent on the valence state of the iron in the ash particles.

The valence state of the iron in the ash particles is influenced by several aspects of the particles' history. Ash particles formed in reducing environments are expected

to have higher ferrous (Fe^{2+}) fractions than ash particles formed in oxidizing environments. Also, the initial valence state of the ash and the rate of reduction or oxidation will effect the final valence state. If some particles do not have time to reach an equilibrium valence state before they solidify then the ash particles will likely have a distribution of ferrous/ferric ratios that depends on the history of each particle.

Goodwin [4] has developed correlations that accurately predict the absorption index, k, in the 1-4 μm range for room temperature slags. In these relations the absorption index is found to correlate with Fe^{2+} content. To use these correlations, one must not only know the iron content, but also the Fe^{2+}/Fe ratio. Mössbauer spectroscopic measurements on individual fly ash particles could, in principle, be used to determine the valence state of ash bound iron, but to our knowledge this has not been done. Vorres [6] suggests that 0.80 is a typical value for the ferrous fraction in coal slags, which is consistent with the values found by Goodwin for synthetic slags.

The conclusion drawn from the above discussion is that we do not know, and are not likely to measure, the valence state of iron in single fly ash particles, since one would have to make measurements for many single ash particles in order to obtain a distribution. Therefore, it is reasonable to assume some average value (e.g. 0.80) for all ash particles. Given the likelihood that fly ash is a relatively poor emitter when compared to other constituents of the coal combustion environment (e.g. H_2O, CO_2, char, and soot), and given the level of uncertainties for other important parameters (e.g. wall emissivities, local ash loading, etc.), this assumption is acceptable. Since k does not vary significantly over the range 1-4 μm, it is further assumed that k in this wavelength range is constant with a value depending only on T and the weight percent of Fe_2O_3.

A correlation for the constant absorption index, k, in the 1-4 μm wavelength range was found for room temperature slags by averaging k over wavelength for the 16 slags studied by Goodwin [4]. The values for k are plotted versus Fe_2O_3 weight percent and a quadratic of the form $ax + bx^2$ was fitted through the points using least squares. Figure 13 shows the data and the best fit

$$k_{avg} \simeq 4.025 \times 10^{-5} x + 1.689 \times 10^{-6} x^2 \tag{14}$$

where x is the weight percentage of Fe_2O_3. The fit is reasonably accurate for most of the the slags, with the expected trend that Eq. (14) underpredicts k_{avg} for highly

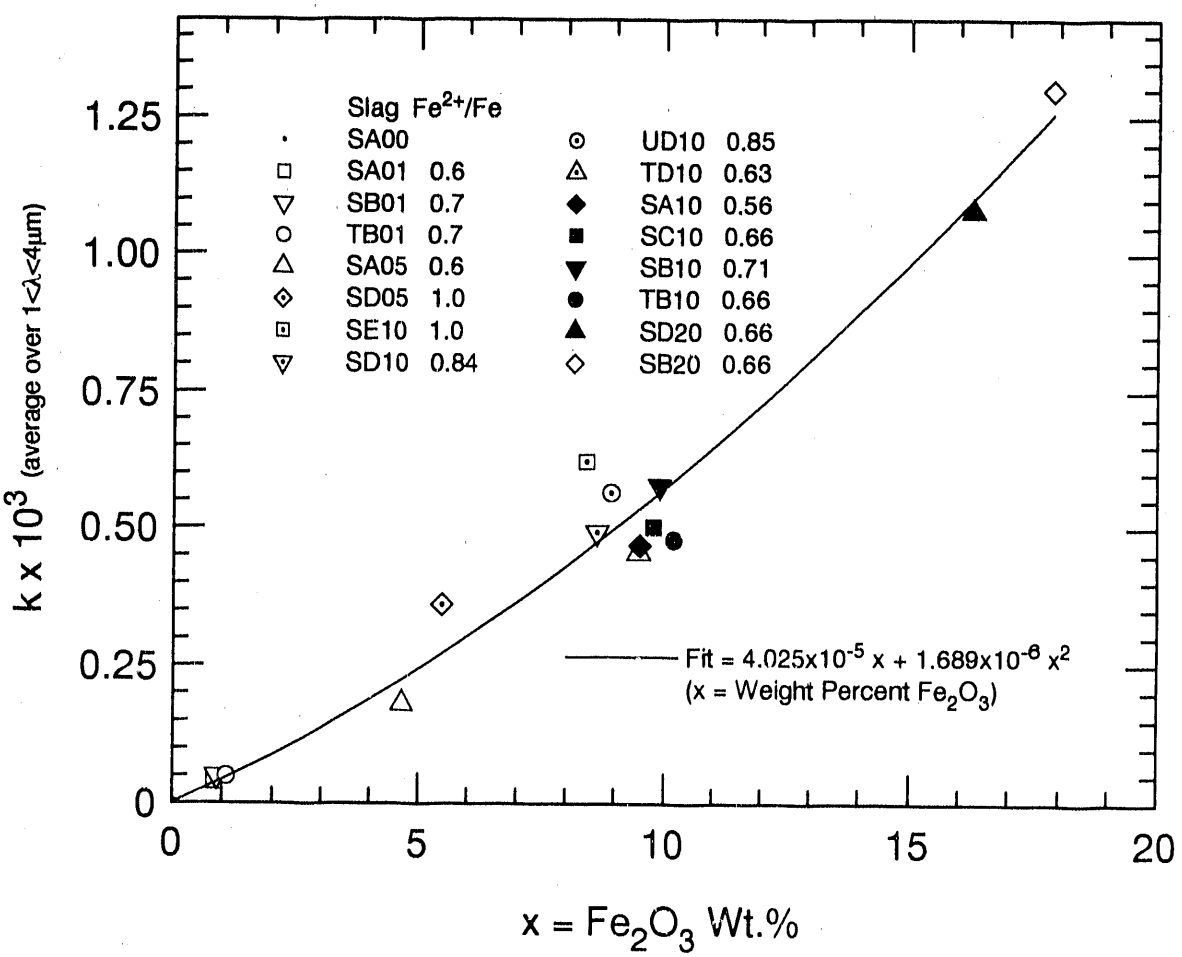

Figure 13: Average k in the 1-4 μm range versus weight percent Fe_2O_3 for several room temperature slags.

reduced slags (e.g. SD05 and SE10) and overpredicts k_{avg} for slags produced in air (e.g. SA05 and SA10). The largest error is for SE10, where Eq. (14) underpredicts k_{avg} by 26%.

Plots of k versus wavelength are shown in Fig. 14 along with the average value, k_{avg}, predicted by Eq. (14). It is evident that the assumption that k is constant over the 1-4 μm range is not unreasonable; however a better test is to compute the absorption efficiency for a distribution of particle sizes and compare the exact and approximate results. This calculation was done assuming a log–normal particle size distribution (see previous QPR) with volume median diameter $\overline{D_3} = 10\mu$m and $\sigma_g = 2.5$. The results are shown in Fig. 15. The exact results (solid line) compare favorably with the

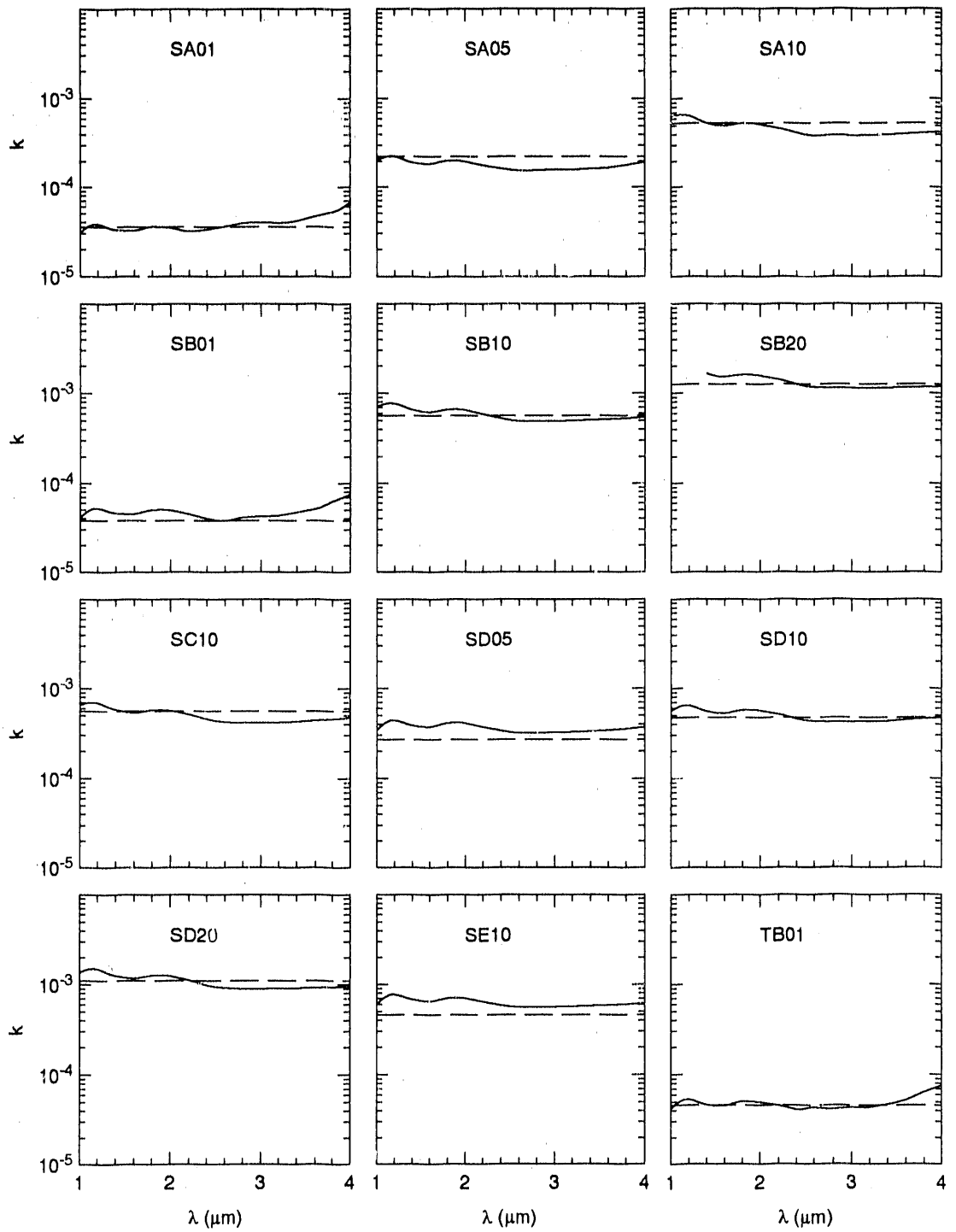

Figure 14: Comparison of k (solid) and k_{avg} for 15 slags at room temperature

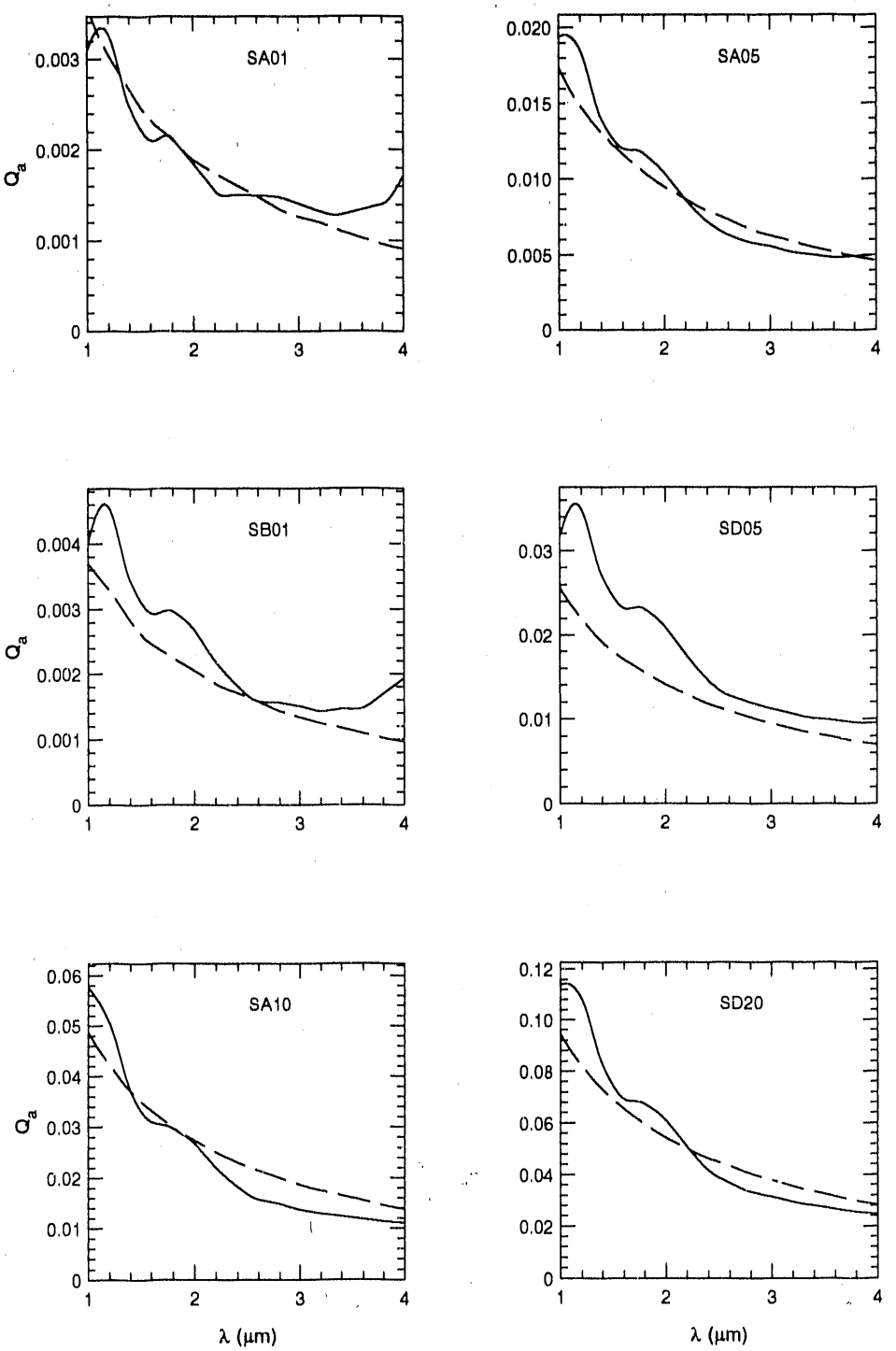

Figure 15: Absorption efficiency versus wavelength for actual k (solid) and approximate k_{avg} (dashed) for a log–normal size distribution with $\overline{D_3} = 10\mu$m and $\sigma_g = 2.5$.

approximate results (dashed line) for most of the slags. The largest errors were for SD05 (middle right) and SE10 (not shown). For most slags the approximation under predicts Q_a at shorter wavelengths and over predicts Q_a at longer wavelengths.

The effect of this approximate model for k in the 1-4 μm range on the total radiative transfer from a dispersion of ash in infrared active combustion gases (CO_2 and H_2O) is being studied to determine if more accurate models for k are necessary. Preliminary results indicate that this model is probably adequate.

3) Oscillator Fits of the Optical Constants for the Range 8< λ <13 μm

In the wavelength range $8 < \lambda < 13\mu$m the complex refractive index is determined by the vibrational absorption by SiO_2. There are three absorption mechanisms that contribute the behavior of m in this region. First, there is a fundamental vibrational absorption peak near 9.4 μm associated with Si-O with bridging oxygen (i.e., Si-O-Si). The second absorption feature centered near 10.4 μm is due to vibration of the non-bridging Si-O^-. A third, smaller absorption feature, lies near 13 μm and is possibly due to ring groups [4].

For room temperature slags, these three absorption mechanisms are all quite visible in the k spectrum. A three oscillator model for the complex dielectric constant, ϵ, of the form

$$\epsilon \equiv m^2 \simeq n_\infty^2 + \sum_{j=1}^{3} \frac{\omega_{pj}^2}{\omega_{0j}^2 - \omega^2 - i\gamma_j\omega} \tag{15}$$

fits experimental measurements quite well [4], with average errors in n and k of approximately ± 0.06. The largest errors were at wavelengths greater than 11 μm where the third oscillator is important. Below 11 μm the first two oscillators are dominant. The peak strengths of the first two oscillators (9.4 μm and 10.4 μm) correlate with iron content. The 9.4 μm peak strength decreases with increasing Fe_2O_3 content and the 10.4 μm peak strength increases with increasing iron. The explanation for this behavior is that addition of non–network forming metal oxides into the glass structure prevents oxygen bridging, thus increasing the Si-O^- absorption and decreasing the Si-O-Si absorption [3]. Note that Fe_2O_3 is not particularly special in this regard since other species, such as CaO or Na_2O, also restrict the Si-O bridging. Also, it appears that increasing the temperature of the slag has a similar effect, as exhibited by the molten slag data presented under Task 2.

In fits presented by Goodwin [4], all of the parameters, including n_∞, were allowed to vary until the best fit was found. However, this makes it difficult to construct simple correlations for m for a large range of compositions unless all the parameters correlate to the same independent variable, such as Fe_2O_3 or SiO_2 content. A less accurate but simpler correlation may be preferable.

During the next quarter, simpler correlations in this wavelength range will be evaluated, with particular attention to relations that can be extended to the higher temperature data. It should be possible to construct accurate but simple correlations in this range which are based on SiO_2 content.

2.3.5 Radiation Transfer Calculations

During this quarter, a number of calculations were made to begin the evaluation of the effects of fly ash on heat transfer in coal combustors. Codes were developed to compute the spectral radiative properties of infrared active gases, CO_2, H_2O, and CO using the exponential wide band model. Using the radiation transfer codes reported in the previous QPR, the total emittance and transmittance is computed for fly ash dispersed in infrared active gases. Several calculations have been done to check the accuracy and validity of the codes.

Table 3 shows results for an isothermal slab of fly ash, CO_2, and H_2O. To compute the gas emission spectrum, the total pressure was assumed to be 1 atm with partial pressures of CO_2 and H_2O of 0.16 and 0.06, respectively, and a slab thickness of 3 m. The radiative properties of the ash dispersion were computed using a log-normal size distribution with volume median diameter $\overline{D_3} = 12$ μm and geometric standard deviation $\sigma_g = 2.5$. The size distribution is truncated outside the diameter range $0.2 \leq D \leq 50\mu$m, which includes over 99% of the ash particle *area*. This distribution has a Sauter median diameter, D_{32}, of approximately 7.47 μm. The total emittance and transmittance were computed and normalized to include only radiation in the wavelength range $1 \leq \lambda < 12.8\mu$m, which is the wavelength range of available ash property data. This wavelength range includes approximately 93% of the total blackbody radiation at 2000 K, with most of the remaining 7% falling below 1 μm.

All of the particles in the ash dispersion were assumed to have the same optical constants in each of the three cases studied. In the first case, the ash particles were

Table 3: Hemispherical emittance, ϵ, and transmittance, τ, of a 2000 K slab of CO_2 (p_{CO_2} =0.16 Atm) and H_2O (p_{H_2O} =0.06 Atm) and fly ash. Slab thickness is 3 m and total pressure is 1 Atm.

$\frac{C_v L}{D_{32}}$	ϵ	τ	$\frac{\epsilon-\epsilon_0}{\epsilon_0} \times 100$	$\frac{\tau-\tau_0}{\tau_0} \times 100$
SA05 ash properties at 20°C				
0	0.264	0.736	0.0	0.0
0.03	0.267	0.710	1.4	-3.7
0.09	0.271	0.664	2.7	-9.8
0.3	0.280	0.553	6.1	-24.9
0.9	0.295	0.376	11.8	-49.0
1.5	0.304	0.278	15.4	-62.2
SA05 ash properties at 1600°C				
0	0.264	0.736	0.0	0.0
0.03	0.268	0.708	1.6	-3.8
0.09	0.273	0.661	3.5	-10.2
0.3	0.287	0.545	8.8	-25.9
0.9	0.314	0.360	19.0	-51.1
1.5	0.333	0.259	26.2	-64.8
SD20 ash properties at 20°C				
0	0.264	0.736	0.0	0.0
0.03	0.271	0.706	2.7	-4.1
0.09	0.281	0.655	6.8	-11.0
0.3	0.314	0.528	19.2	-28.3
0.9	0.385	0.322	46.2	-56.3
1.5	0.436	0.211	65.4	-71.4

assumed to have optical constants of slag SA05 at 20°C. In the second case the ash particles were assumed to have optical constants of slag SA05 at 1600°C, and in the third case the optical constants were assumed to be those of slag SD20 at 20°C, a slag containing approximately 16 weight percent Fe_2O_3 and produced in a reducing atmosphere. The low temperature slag properties are from Goodwin [4] and the high temperature properties are results from Task 2.

Gas optical properties were computed using the exponential wide band model presented by Edwards [7]. Each spectral band is assumed to have a constant transmittance, τ_λ, across its width, which is computed assuming a gas pathlength equal to the width of the

slab, L. From τ_λ a spectral absorption coefficient, α_λ, is computed using the approximation $\tau_\lambda \simeq \exp(-\alpha_\lambda L)$. Then the absorption coefficients of overlapping gas bands and the fly ash are added to give the spectral absorption coefficient of the uniform slab.

Results were compared to calculations by Goodwin [8] and found to be in excellent agreement, despite the fact that Goodwin used a narrow band model [9] for the gas optical properties having considerably more spectral detail. No attempt was made to correct the gas radiation properties for the possible effects of increased pathlength due to scattering. For purposes of determining the effects of fly ash on radiative transfer through coal combustion products, the considerable effort involved in such a correction is not justified.

The radiation transport equation was solved at approximately 100 spectral locations (combined ash plus gas spectral data) for each ash loading parameter ($C_v L/D_{32}$) using the discrete ordinates codes discussed in the previous QPR. The anisotropic scattering phase function was modeled as a forward delta function plus a 5th order Legendre polynomial series (see previous QPR). The spectral hemispherical emittance and transmittance were integrated over wavelength (convolved with the Plank blackbody function at 2000 K) to yield the total hemispherical emittance and transmittance.

Upon examination of Table 3, it is clear that ash can significantly affect the radiation transfer in a coal combustor, particularly at high ash loading ($C_v L/D_{32}$). For this isothermal slab the emittance increases by as much as 26% due to SA05 ash emission. It is also evident that using the optical constants of high temperature slag produced significantly higher emission than does using low temperature optical constants.

The largest effect of ash is to reduce the transmittance of the dispersion. The transmittance of this 3m ash layer is reduced by 60-70% at the highest ash loading considered. Even moderate ash loading ($C_v L/D_{32}$=0.3) reduces the transmittance by more than 20%.

The third case in Table 3 is computed assuming the optical constants of the ash particles are those of synthetic slag SD20. Slag SD20 is similar to the SAxx slags except it was produced in a reducing atmosphere. The measured Fe_2O_3 content is approximatly 16.5 wt.%. Even though most (by volume) ash particles have lower Fe_2O_3 content that this, if Fig. 12 is representative of most ashes, it is interesting to see the effect of such high iron content on the emittance. The emittance increase due to

the ash is quite important ($\sim 50\%$) for an ash loading parameter, $C_v L/D_{32}$, as low as 0.9. The decrease in the transmittance due to ash, which is primarily due to scattering, is not affected as much.

The results shown in Table 3 demonstrate the current computational capabilities and demosntrate that ash can significantly influence the total emittance and transmittance of a hot layer of emitting gases. Emission by ash, primarily in the short wavelength region where the Fe_2O_3 content is important, increases the total emittance. Scattering by the ash decreases the transmittance of the ash layer.

2.3.6 Ash Loading in Coal Combustors

It is evident from the previous section that the ash loading parameter, $C_v L/D_{32}$, is a very important parameter for determining the effect of fly ash on radiation heat transfer in a coal combustion environment. Therefore, a simple calculation is presented which estimates the ash loading for various combustion conditions and coal properties.

The ash loading in a coal combustor is dependent on a number of factors including the ash content of the original coal, the fuel bound oxygen content, and the amount of excess air for combustion. Also, since the density of the gaseous products is proportional to P/T, the average ash volume fraction is also proportional to P/T.

The partial pressures of CO_2, H_2O, and CO in the combustion products are also dependent on the original coal composition, and to a lesser extent on pressure and temperature through chemical equilibrium considerations.

For purposes of determining approximate average values of the ash volume fraction, C_v, and H_2O and CO_2 partial pressures in typical coal combustion products, the coal combustion reaction is assumed to be

$$(n_C C + n_H H + n_O O) + n_{air} f O_2 + n_{air}(1-f) N_2 \rightarrow n_{CO_2} CO_2 + n_{H_2O} H_2O + n_{air}(1-f) N_2 \quad (16)$$

where n_i is moles of species i and f is the volume fraction of oxygen in the "air", typically 0.21. The elemental composition of coal varies somewhat with rank and seam, but is primarily carbon, hydrogen, oxygen, and ash (all the inert minerals in coal). Elemental analysis [10] of several coals is presented in Table 4. For purposes of establishing ash loading the sulfer content of the coal is ignored and the coal is assumed

to be dry. The ash content varies from 5 to 20 percent for the coals shown. Also, since high levels of fuel bound oxygen decreases the air demand, the ash volume fraction may be slightly higher for coals with more oxygen.

Table 4: Coal composition analysis for several U.S. Coals [10]

			Elemental Weight Percent				
Seam	State	Rank	C	H	O	S	Ash
Upper Freeport	PA	Med. Vol. Bit.	86	4.7	8	2.3	13
Wyodak-Anderson	WY	Subbituminous	75	5.4	18	0.6	9
Illinois #6	IL	High Vol. Bit.	78	5.0	14	4.8	15
Pittsburgh #8	PA	High Vol. Bit.	83	5.3	9	2.2	9
Pocahontas #3	VA	Low Vol. Bit.	91	4.4	2	0.7	5
Blind Canyon	UT	High Vol. Bit.	81	5.8	12	0.6	5
Lewiston-Stockton	WV	High Vol. Bit.	83	5.3	10	0.7	20
Beulah-Zap	ND	Lignite	73	4.8	20	0.8	10
Notes: C, H and O are on moisture and ash free basis S and Ash are on dry basis							

The mole fractions of the products in Eq. (16) are found assuming $f = 0.21$ and 10% excess air. The density and mass of the resulting gaseous products (ρ_{gas} and x_{gas}) are computed assuming an ideal gas mixture. The ash volume fraction is computed using the relation

$$C_v \simeq \frac{x_{\text{ash}}/\rho_{\text{slag}}}{x_{\text{gas}}/\rho_{\text{gas}}} \tag{17}$$

where x_{ash} is the mass of ash (per unit mass of coal), ρ_{slag} is the density of the ash particles (assume 2.5 g/cm^3). It is also assumed that the slag density is much higher than the gas density.

Results of the analysis are shown in Fig. 16 for a temperature of 2000 K and total pressure of 1 atm. The volume fraction, C_v, is of the form

$$C_v \sim \frac{x_{\text{ash}}}{1 - x_{\text{ash}}} \frac{P}{T}. \tag{18}$$

The solid curve was computed for coal carbon, hydrogen, and oxygen weight percentages of 75, 5, and 10, respectively. The dotted curves show results for coal compositions from Table 4. In Fig. 16, the ash volume fraction, C_v, is approximately 1.5×10^{-6} for high ash coal ($x_{\text{ash}} \sim 20\%$).

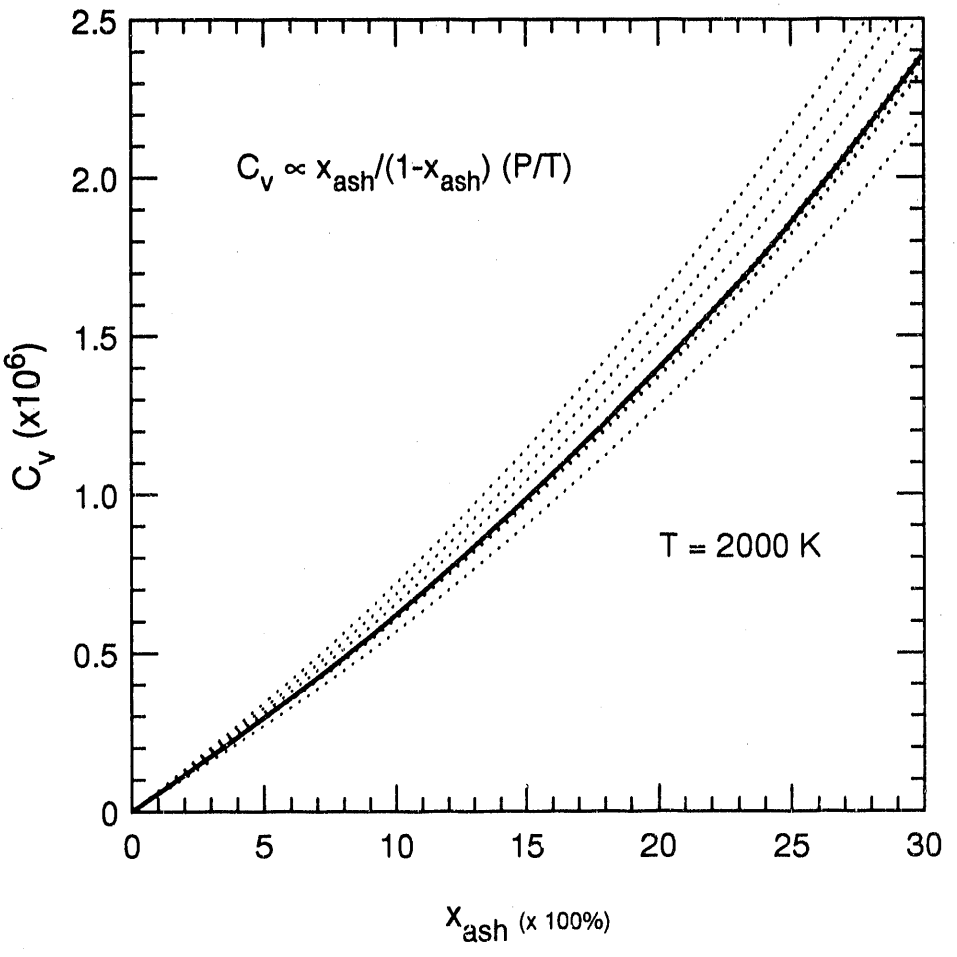

Figure 16: Ash volume fraction versus mass fraction of ash in the coal, x_{ash}, at T=2000K and P=1atm. The solid curve is for coal (C,H,O) mass fractions of (75,5,10) weight percent. The dashed curves are for coals in Table 4.

Consider the radiation transfer calculations discussed in the previous section. The size distribution had a Sauter mean diameter, D_{32} of approximately 7.47 μm and the slab thickness was 3m. Therefore, for approximately 20% ash in the coal the ash loading parameter, $C_v L/D_{32}$, is approximately 0.6. At this value of $C_v L/D_{32}$ the hemispherical emittance is increased approximately 14% due to fly ash if all the ash is SA05 (using high temperature optical constants). The transmittance of such a layer is decreased by approximately 38%. Note that this is for a 3m slab – the distances between the hot sections of a combustor and the superheat tubes might be 5-10 times this large. If the

3m layer is cooler, say 1500 K, then $C_v L/D_{32}$ will be approximately 0.9, and the ash decreases the transmittance by a factor of approximately two.

Consider the low ash loading case in which the coal contains 5% ash by mass. The ash volume fraction is approximately 0.25×10^{-6} and for $L = 3$m and $D_{32} = 7.47$ μm, the ash loading parameter, $C_v L/D_{32}$, is only 0.1. Referring to Table 3, the hemispherical transmittance is decreased by approximately 10% due to the ash. The emittance is only increased by approximately 4% for the SA05 ash.

2.3.7 Summary

During the past quarter considerable progress has been made. A classification scheme was proposed for computing the average scattering and absorption properties of fly ash dispersions. Correlation formula for the optical constants of coal slags were presented that make use of this classification scheme. Efforts to find simple correlations that include temperature effects continue.

Computer codes were written that combine average spectral radiation properties for ash dispersions with gas radiation properties (CO_2, H_2O, and CO). These combined properties are input for radiative heat transfer codes that solve the transport equation through planar slabs of gas/particle dispersions to obtain the total transmittance and emittance. Preliminary results for simplified ash distributions with uniform particle composition were presented, and indicated that ash does significantly effect the radiation transfer. High ash loading enhances the emittance of an isothermal slab and reduces its transmittance by as much as 50% or more. Even low ash loading can significantly decrease ($\sim$ 10%) the transmittance of a 3 m slab of CO_2 and H_2O.

During the next quarter efforts will focus on completing Task 2 so that correlations can be obtained that include temperature effects. These correlations will be used along with CCSEM composition distribution results to evaluate the effects of fly ash on heat transfer through isothermal planar slabs and on slabs with a temperature distribution.

2.4 Task 4: Measurement of the Radiant Properties of Fly Ash Dispersions:

In this Task, a bench-scale experiment under controlled conditions in the laboratory is to be performed to test the validity of the approach taken in the first three Tasks. Measurements of extinction of infra-red radiation in the wavelength range of 1-12 μm by a well-dispersed suspension of fly ash, of known loading and in suitably transparent liquids, are to be made at room temperatures. As discussed in the QPR dated October 1989, the liquids to be used in different wavelength ranges are carbon tetrachloride (CCl_4), carbon disulfide (CS_2) and bromoform ($CHCl_3$). In the wavelength range 1-5 μm, sapphire windows 1 mm thick are being used. Beyond 5 μm, the transmittance of the sapphire window falls sharply and barium fluoride (BaF_2) windows of thickness 2 mm are used in the range of 5-12 μm. The reason for using sapphire windows in the low wavelength range is that they are more resistant to scratches and are relatively cheaper to replace in case of damage than the BaF_2 windows.

A schematic of the cell is shown in Figure 1. The 2" diameter windows cover both the test cell containing the dispersed ash and the reference cell containing the pure liquid. Thus the signal passing through both the dispersion and the reference signal are measured under the same conditions. Two pairs of Viton O-rings are used to seal the cells. The output shaft of the small 12 V motor, mounted on the top of the cell, is coupled to the glass stirrer. The stirrer is operated at a speed high enough to prevent heavy particles from settling, but without generating bubbles. The thickness of the slab of suspension, between the two windows, is 9 mm. The cell is screwed on to an optical post as shown.

Figure 2 is a schematic of the experimental set-up. At each wavelength, the transmittance is determined by computing the ratio of the signal passing through the test cell to that passing through the reference cell. The optical post on which the cell is mounted is moved transversely on an optical rail so that the test and the reference cells can be moved into the path of the beam successively. Stops are used on the optical rail to ensure that the beams pass through the same spots on the cell windows.

The optical configuration and most of the components of the experimental apparatus are same as those used in Task II. They are described in detail in pages 45 and 46 of the QPR dated April, 1988, but are repeated here for the reader's convenience. The broad-band infra-red source is a Nernst glower. The ceramic glowbar, 1 mm in diameter, is heated to a brightness temperature of ~2000K. An aperture, 2 mm wide, is positioned at the focal point (see Figure 2) so that the diameter of the beam passing through the cell is approximately 5 mm. The reference signal for the lock-in amplifier (Stanford Research Systems, Model SR-530) is

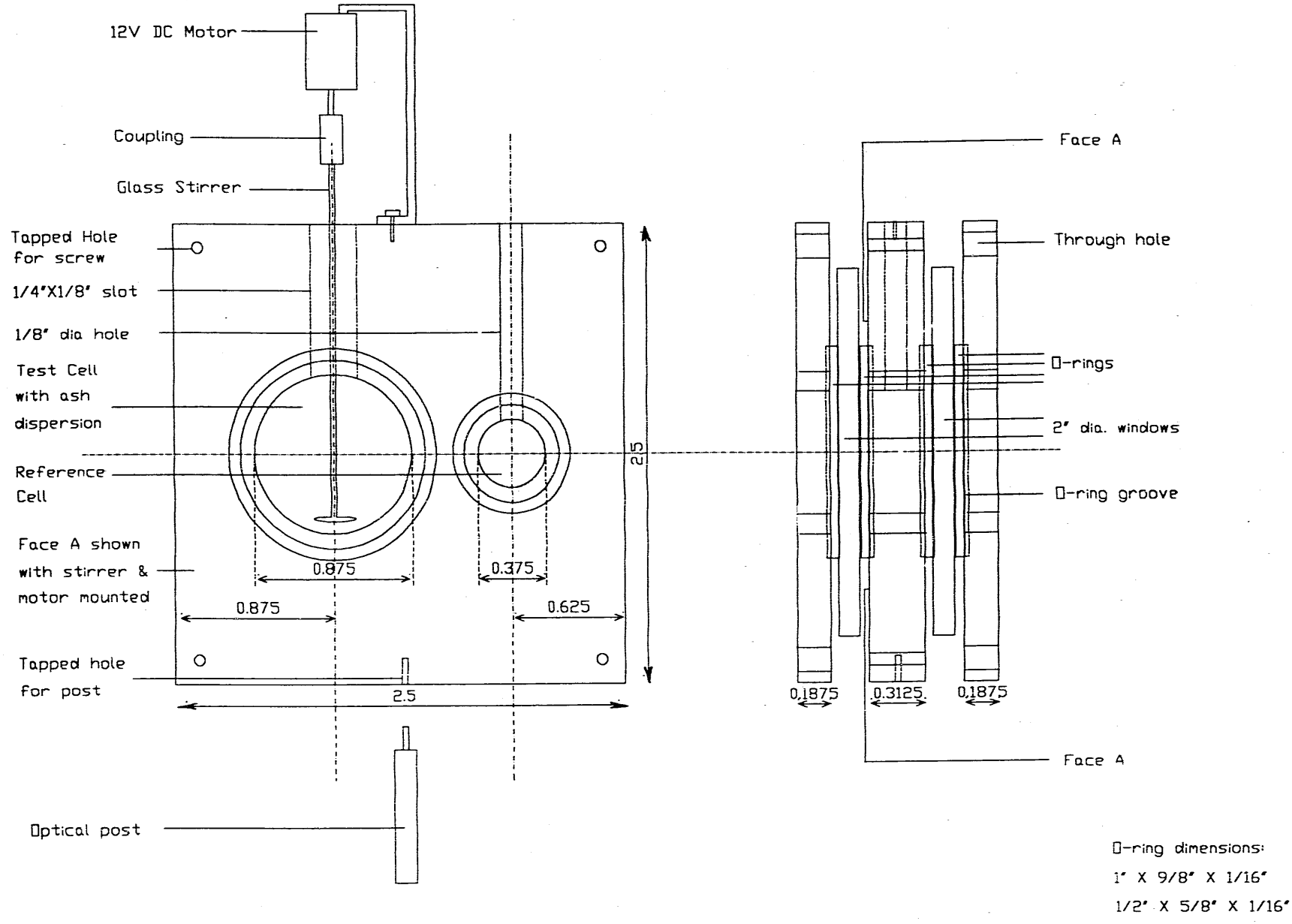

Figure 1. Experimental Cell for Task IV Measurements

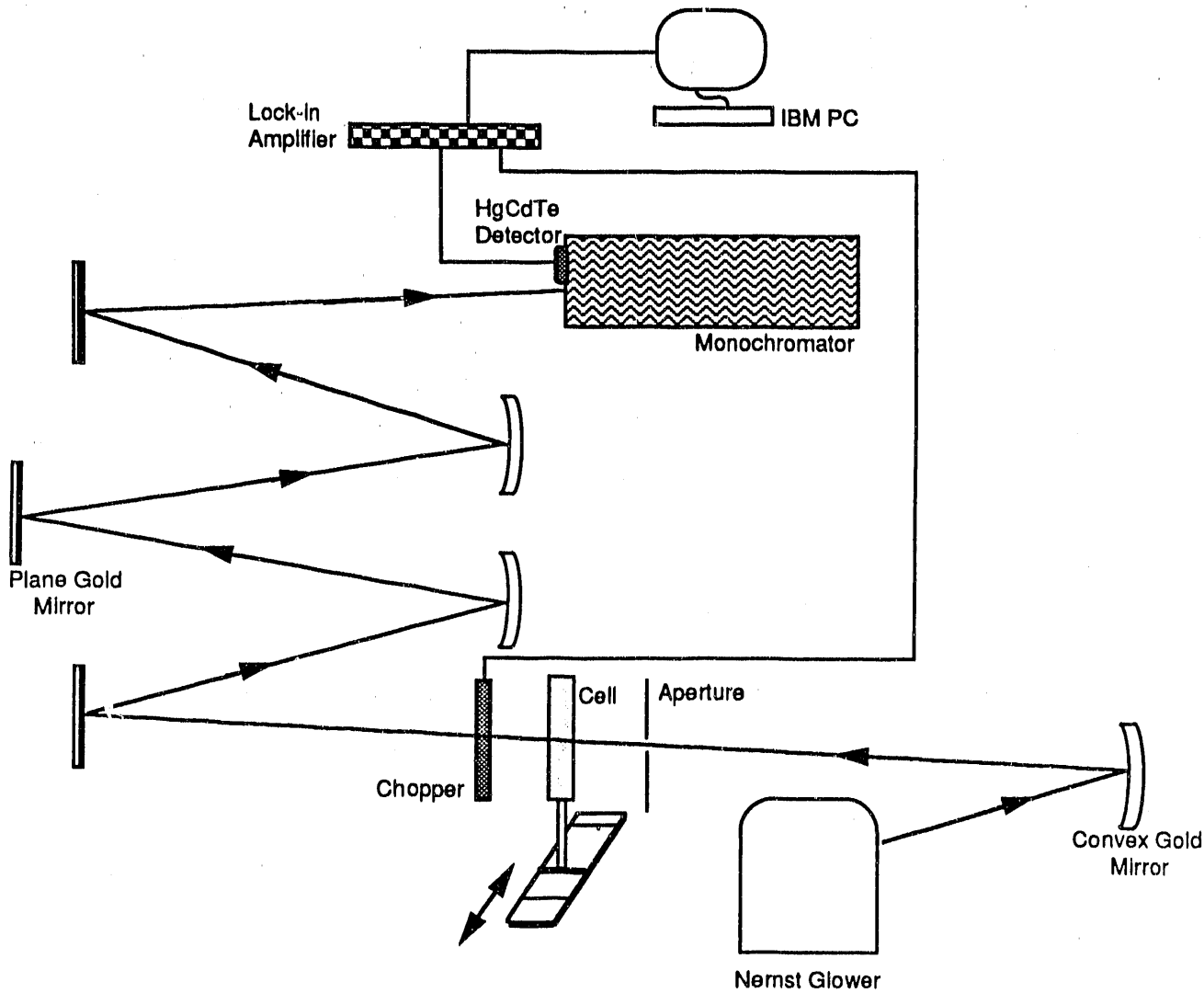

Figure 2: Experimental Set-up

provided by the mechanical chopper which modulates the beam from the glower at 670 Hz. This phase-sensitive detection system is used to reject background radiation by trading bandwidth for signal-to-noise ratio. The gain and the integration time of the amplifier can be set by the computer-controlled data acquisition system. A number of front-surfaced gold mirrors, both flat and concave, are used to focus and re-direct radiation from the glower to the 1 mm wide entrance slit of the monochromator (Ebert-type, F#8.6). Four sets of gratings are used to spectrally resolve the signal from the visible through the infra-red to 14 μm.

Many tests were performed on the latest design of the experimental cell, and others are currently in progress. One of the first tests was to measure the ratio of the transmittances of the test cell to that of the reference cell, with both containing CCl_4 only. Ideally, this ratio should be 1.0. The wavelength range of 1.0-1.5 μm was chosen for all the test measurements because there are no major CCl_4 absorption bands in this region. As described later, accurate measurements are difficult in wavelength ranges where the dispersing medium is strongly absorbing. Figure 3 shows the results for a series of scans. With few exceptions, the ratio is well within 1.0% of unity. Such a small error is acceptable.

The next step was to test the measurement process for repeatability. It was quickly apparent that unless measures were taken to seal the test cell adequately, steady evaporation of CCl_4 resulted in an increase of the ash volume fraction C_v, and hence an increase in the extinction. With proper sealing, the transmitted signal remained quite steady over a period of almost an hour. However, over longer periods of several hours, small amounts of ash are lost from the dispersion when they are trapped in the gap between the cell wall and the window around the O-rings. This increases the transmittance. We have not yet overcome this problem. By adding just enough ash suspension of the same loading to increase the extinction at a fixed wavelength to the same value as that at the beginning of the experiment, it was found that the extinctions at other wavelengths were within the current range of precision. This reproducibility could mean that the particles are lost almost randomly, independent of size. Still, it is preferable to find a way to prevent a loss of particles from the dispersed state. Figure 4 shows results of repeated scans with three different loadings. The current range of repeatability appears to be within 2-3%.

So far we were only interested in obtaining extinctions over desired ranges without accurately measuring the ash loadings. Experiments with pre-determined ash loadings will be performed with controlled loadings obtained by the method described below.

Preparation of fly ash suspension: To obtain a desired ash loading, a sample of fly ash, whose mass can be measured to an accuracy of 0.1 mg, is added to any of the liquids. The mass of the latter can be measured to an accuracy of 0.1 gm. For example, we can use

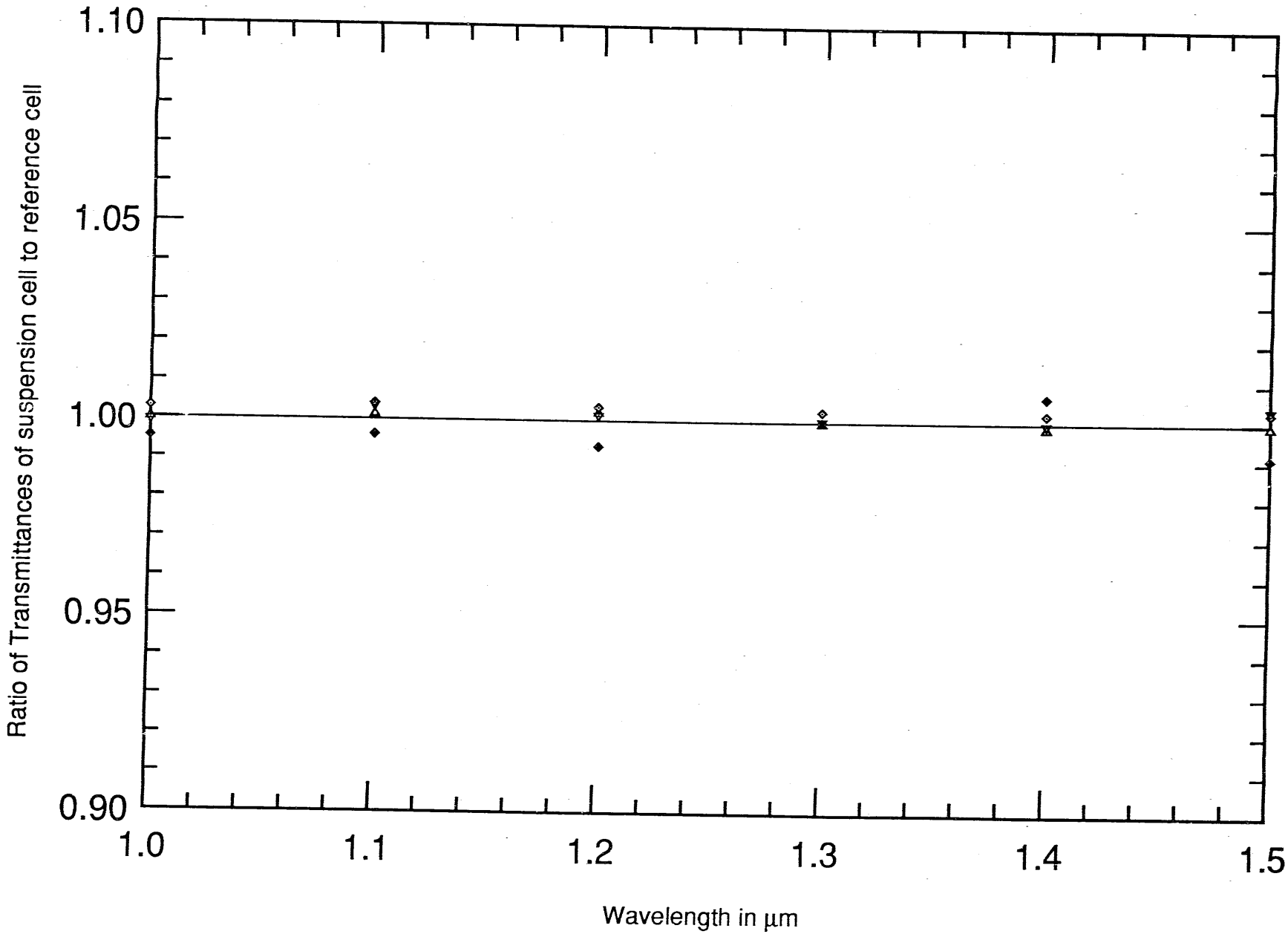

Figure 3. Tests on Experimental Cell for Task IV

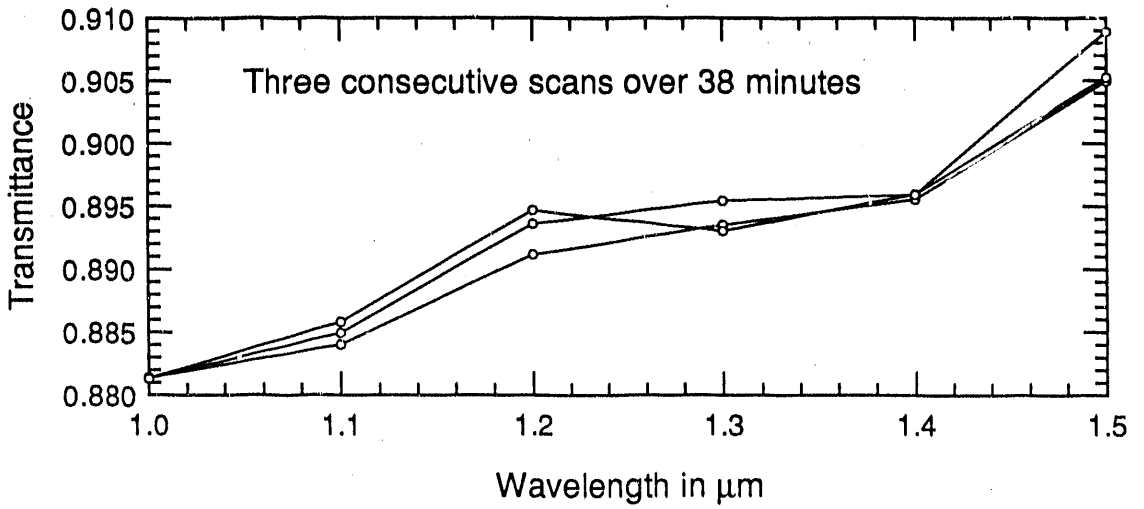

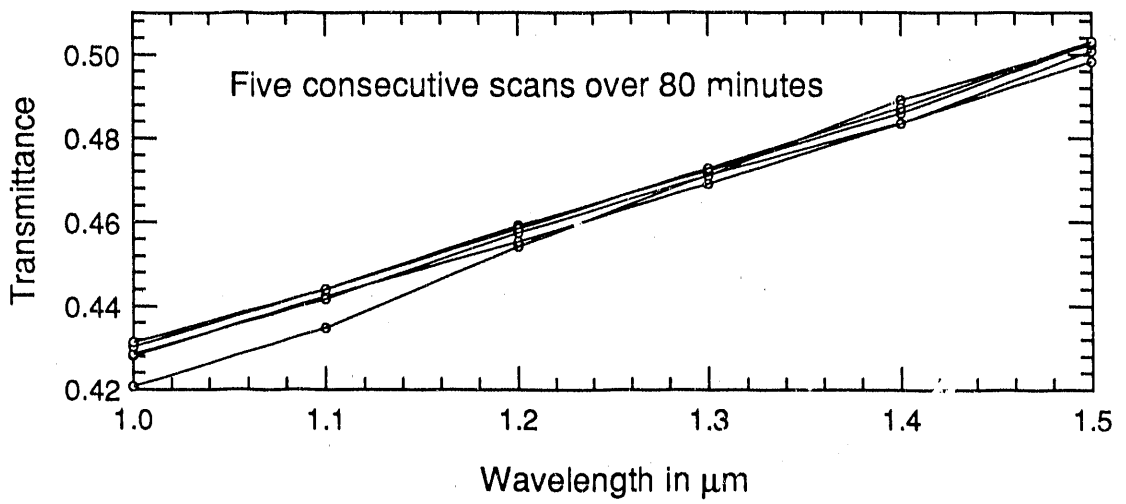

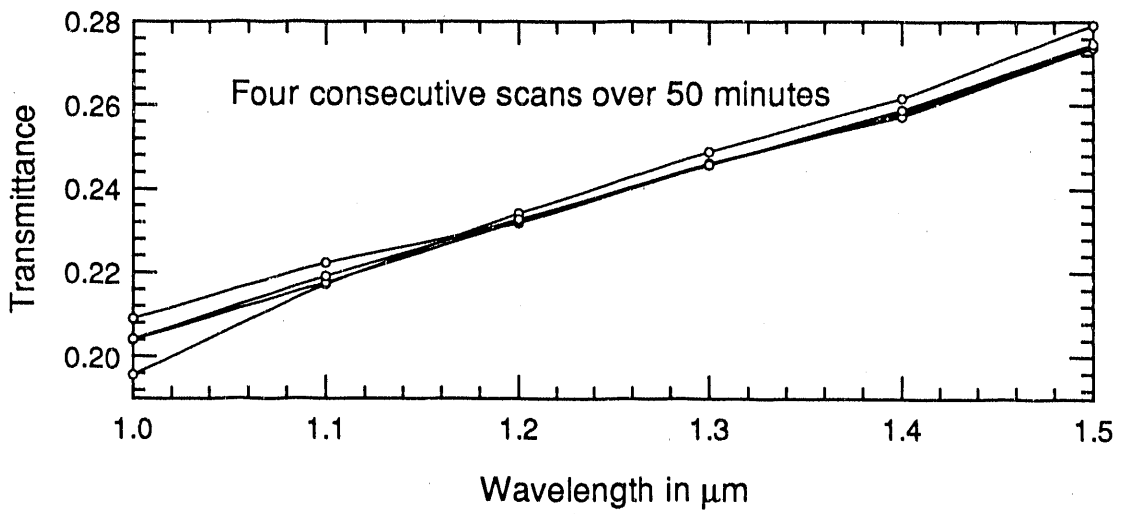

Figure 4: Repeated transmittance measurements for various fly ash loadings

40 mg of Upper Freeport ash in 100 ml of CCl_4. These values yield an uncertainty in the mass fraction of the ash, C_m, of 0.3%. However, the volume fraction of ash, C_v, is needed for calculations in Task 3. The density of pure CCl_4 at room temperature is known to an accuracy of 1.5940 g/cc [Reference 2]. Since we are using 99.0% pure CCl_4, we know its density to 1.0% accuracy. The average density of the ashes will be accurately determined next quarter using a specific gravity bottle and the same procedure used earlier in measuring the density of slags (see page 8, QPR dated April, 1990).

The ash suspension of a fixed loading thus prepared is stored in a glass bottle sealed with a cap. Later, if necessary, additional liquid can be added to raise the value of the total mass (of the liquid, ash and bottle) to the value which was noted at the time of storage. The suspension in the bottle is ultrasonically agitated before withdrawing a sample using a pipette.

Other activities scheduled for the immediate future include determining maximum loading limit for single scatter and selecting the exact wavelength ranges over which the transmission measurements will be made in the three different liquid media.

3.0 REFERENCES

1. "Transformation of Inorganic Coal Constituents in Combustion Systems," PSI Technology Company, Phase 1, Final Report Draft, March, 1990.

2. *CRC Handbook of Chemistry and Physics*, CRC Press, West Palm Beach, FL, 59th edition.

3. Simon, I., "Infra-red studies of glasses," in *Modern Aspects of the Vitreous State*, J. D. MacKenzie (Ed.), Butterworths, Washington, 1960.

4. Goodwin, D. G., "Infrared Optical Constants of Coal Slags," Ph.D. Thesis, Topical Report T-255, High Temperature Gasdynamics Laboratory, Mechanical Engineering Department, Stanford University, 1986.

5. Born, M. and Wolf, E., *Principles of Optics*, (sixth edition), Pergamon Press, Oxford, 1980.

6. Vorres, K. S., "Effect of composition on melting behavior of coal ash," Journal of Engineering for Power **101**, 497-499, 1979.

7. Edwards, D. K., "Molecular gas band radiation," Adv. Heat Transfer **12**, 115-193, 1976.

8. Goodwin, D. G. and Mitchner, M., "Flyash radiative properties and effects on radiative heat transfer in coal-fired systems," Int. J. Heat Mass Transfer **32**, No. 4, 627-638, 1989.

9. Ludwig, C. B., Malkmus, W., Reardon, J. E., and Thomson, J. A. L., *Handbook of Infrared Radiation from Combustion Gases*, NASA SP-3080, National Aeronautics and Space Administration, Washington, DC, 1973.

10. *Users Handbook for the Argonne Premium Coal Sample Program*, Argonne National Laboratory, Argonne, Illinois, October 1989.

-END-

DATE FILMED

01 / 29 / 91